This is the peer reviewed version of the following article: Huang, W., Wu, T., Xie, C., Rayner, C. K., Priest, C., Ebendorff-Heidepriem, H., J. (T.), , Sensing Intra- and Extra-Cellular Ca2+ in the Islet of Langerhans. Adv. Funct. Mater. 2022, 32, 2106020, which has been published in final form at https://doi.org/10.1002/adfm.202106020. This article may be used for non-commercial purposes in accordance with Wiley Terms and Conditions for self-archiving.

Sensing intra- and extracellular Ca^{2+} in the islet of Langerhans

Weikun Huang, Tongzhi Wu, Cong Xie, Christopher K. Rayner, Craig Priest, Heike Ebendorff-Heidepriem, Jiangbo (Tim) Zhao**

W. H., A/Prof. T. W., C. X., Prof. C. K. R.
Adelaide Medical School, Centre of Research Excellence in Translating Nutritional Science to Good Health, the University of Adelaide, Adelaide, South Australia 5005, Australia
E-mail: tongzhi.wu@adelaide.edu.au

W. H., Prof. H. E., J. (T) Z.
Institute for Photonics and Advanced Sensing, School of Physical Sciences, ARC Centre of Excellence for Nanoscale BioPhotonics, University of Adelaide, Adelaide, South Australia 5005, Australia
E-mail: jiangbo.zhao62@gmail.com

A/Prof. C. P.
Australian National Fabrication Facility and Future Industries Institute, UniSA STEM, University of South Australia, Mawson Lakes, South Australia 5095, Australia

J. (T.) Z.
Department of Engineering, Faculty of Science and Engineering, University of Hull, Hull HU6 7RX, UK

* Author to whom any correspondence should be addressed.

Keywords: Ca^{2+} oscillation; Ca^{2+} signalling; insulin secretion; Ca^{2+} sensors; islet of Langerhans;

Abstract

Calcium ions (Ca^{2+}) take part in intra- and intercellular signalling to mediate cellular functions. Sensing this ubiquitous messenger is instrumental in disentangling the specific functions of cellular sub-compartments and/or intercellular communications. In this review, we first describe intra- and intercellular Ca^{2+} signalling in relation to insulin secretion from the pancreatic islets, and then outline the development of diverse sensors, e.g., chemically synthesized indicators, genetically encoded proteins and ion-selective microelectrodes, for

intra- and extracellular sensing of Ca^{2+}. Particular emphasis is placed on emerging approaches in this field, such as low-affinity Ca^{2+} indicators and unique Ca^{2+}-responsive composite materials. We conclude by remarking on the challenges and opportunities for further developments in this field, which may facilitate a more comprehensive understanding of Ca^{2+} signalling within and outside the islets, and its relevance in health and disease.

1. Ca^{2+} homeostasis and signalling

The homeostasis of calcium ions (Ca^{2+}, free ionic form unless specified) is critical to a range of cellular functions,[1] including endocrine and exocrine secretions[2] gene expression,[3] muscle contraction,[4] fertilization,[5] and neuronal activity.[6] As a ubiquitous messenger, Ca^{2+} is pivotal to transmitting cascade signalling within and between cells, thus coordinating complex cellular activities in response to internal and/or external stimuli. During these processes, there are coordinated exchanges of Ca^{2+} between cellular sub-compartments or among cells, leading to dynamic changes in Ca^{2+} concentration ($[Ca^{2+}]$) in varying domains. As shown in **Figure 1a**, in the resting state, the cytoplasmic concentration of Ca^{2+} ($[Ca^{2+}]_c$) is maintained at about 50~100 nM via plasma membrane Ca^{2+} transport ATPase (PMCA)[7] and Na^+/Ca^{2+} exchanger (NCX)[8]; both export Ca^{2+} from the cytoplasm to the extracellular domain. Ca^{2+} concentrations in the mitochondria ($[Ca^{2+}]_{mito}$) and nucleus ($[Ca^{2+}]_n$) are comparable (0.1-100 μM). Ca^{2+} in the endoplasmic reticulum (ER) ($[Ca^{2+}]_{ER}$) (or sarcoplasmic reticulum (SR) in the case of muscle cells), approximates up to ~500 μM, reflecting its reservoir role for Ca^{2+} inside cells.[9] The concentration of extracellular Ca^{2+} ($[Ca^{2+}]_{ex}$) can reach around 1 mM, i.e. four orders of magnitude higher than $[Ca^{2+}]_c$.[10] Upon stimulation, influx of extracellular Ca^{2+} into the cytoplasm, via plasma membrane Ca^{2+} channels and release of Ca^{2+} from the ER (or SR) via the 1, 4, 5-triphosphate receptor (IP3R)[11] and ryanodine receptor (RyR)[12], leads to

temporary rises of $[Ca^{2+}]_c$ up to 1 μM. The elevated $[Ca^{2+}]_c$, in turn, re-establishes a concentration equilibrium, by extruding Ca^{2+} back into the extracellular domain or refilling the ER (or SR) and mitochondria via Sacro/Endoplasmic Reticulum Ca^{2+}-ATPase (SERCA)[13] and the mitochondrial Ca^{2+} uniporter (MCU)[14], respectively.

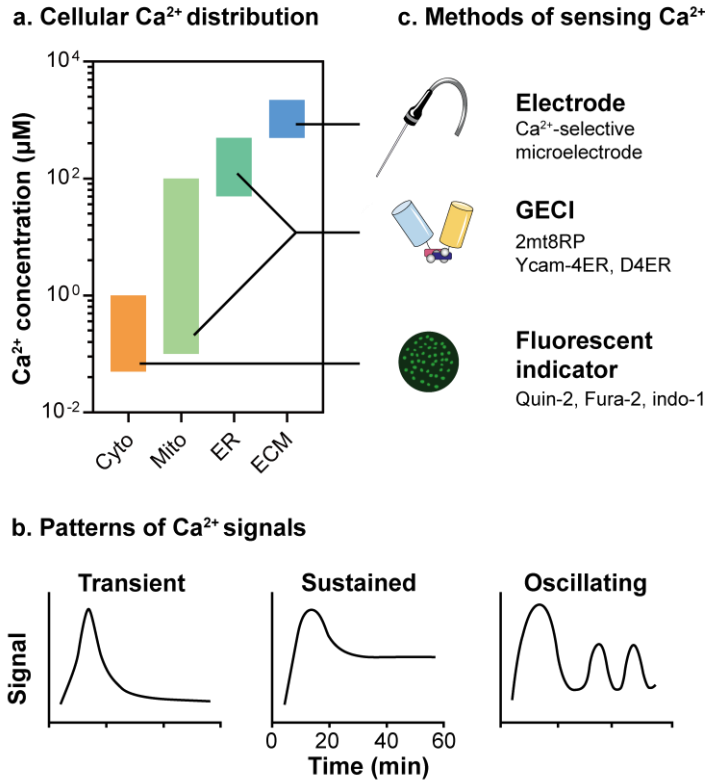

Figure 1 | Cellular Ca^{2+} concentrations, signal patterns and sensors commonly used in islet studies. a | Overview of typical $[Ca^{2+}]$ in intra- and extracellular domains, including Ca^{2+} in the cytoplasm (Cyto, 50-1000 nM), mitochondria (Mito) and nucleus (N, 0.1-100 μM), endoplasmic reticulum (ER, 50−500 μM), and extracellular matrix (ECM, 1 mM);[15] **b |** Schematics of three representative types of cytoplasmic Ca^{2+} signals: transient (left), sustained (middle) and oscillating (right) patterns; **c |** Sensing tools commonly used for measuring Ca^{2+} in islet studies, including Ca^{2+}-selective microelectrodes for extracellular Ca^{2+}, genetically encoded Ca^{2+} indicator (GECI) protein-based indicators (e.g. 2mt8RP for mitochondrial Ca^{2+}, Ycam-4ER and D4ER) for endoplasmic reticulum Ca^{2+}, and fluorescent Ca^{2+} indicators (e.g. Quin-2, Fura-2 and Indo-1) for cytoplasmic Ca^{2+}.

Within the cytoplasm, variations in Ca^{2+} signals appear in transient, sustained or oscillatory patterns (Figure 1b), in the context of physiological or pathological processes.[16] The transient increase in $[Ca^{2+}]_c$ reflects a rapid influx of extracellular Ca^{2+} through Ca^{2+}-permeable channels in response to cellular depolarization, followed by prompt and effective Ca^{2+} transport into

other intra- or extracellular compartments (described in the preceding paragraph). The latter drives $[Ca^{2+}]_c$ to return to its original level in a short timeframe to avoid overloading of Ca^{2+}.[17] Accordingly, any impairment in this process may result in prolonged elevation of $[Ca^{2+}]_c$, leading to programmed cell death or necrosis.[18] Physiological cellular responses to continued stimulation are therefore associated with oscillatory changes in $[Ca^{2+}]_c$, as well as $[Ca^{2+}]$ in other intra- and extracellular domains, although the pattern may be atypical in many instances.[19]

Following the discovery that skeletal muscle contraction is linked to coordinated, and repeated, changes in $[Ca^{2+}]_c$,[20] Ca^{2+} oscillations have since been recognized as a universal mechanism underlying many biological events, such as egg fertilization,[21] insulin secretion from pancreatic β cells,[22] and interleukin production from macrophages.[23] In this review, we first discuss the relevance of intra- and intercellular Ca^{2+} signalling based on the function of pancreatic islets, particularly the phenomenon of a pulsatile insulin response to glucose. We then outline the chronological development of Ca^{2+} sensing methodologies (Figure 1c) that are critical to the in-depth understanding of these physiological processes in the islets, where we remark on the rationale (pros and cons) for the selection of prevalent and emerging indicators, as well as the analytical techniques/platforms in the context of various applications. We finally provide an outlook on the prospects of Ca^{2+} sensing in the study of islets and in broader biomedical research, highlighting the challenges and opportunities.

This review is not intended to be exhaustive, but instead emphasizes the sensing techniques for detection/monitoring of dynamic cellular Ca^{2+} concentrations and associated secretory activity. Accordingly, measurement of non-labile calcium (i.e. calcium tightly incorporated within cellular structures) is beyond the scope of this work. The extensive range of chemical and protein-based Ca^{2+} sensors and corresponding sensing mechanisms has been summarized elsewhere,[24] and will not be specifically discussed. We anticipate that knowledge relevant to

the development and selection of Ca^{2+} sensors in islet studies will be applicable to a broad range of research interests, such as monitoring of neuronal activity, cardiovascular functions and cancer development.[25]

2 Insulin secretion and Ca^{2+} signalling

2.1 Pancreatic islets and pulsatile secretion of insulin

The pancreatic islet is a miniaturized endocrine organ that comprises α, β and δ cells, responsible for the secretion of glucagon, insulin and somatostatin, respectively. As illustrated in **Figure 2a**, these three endocrine cells are distributed in a scattered fashion in the human islet, but exhibit region-specific distribution in the mouse islet (with β cells condensed in the core and surrounded by other cells).[26]

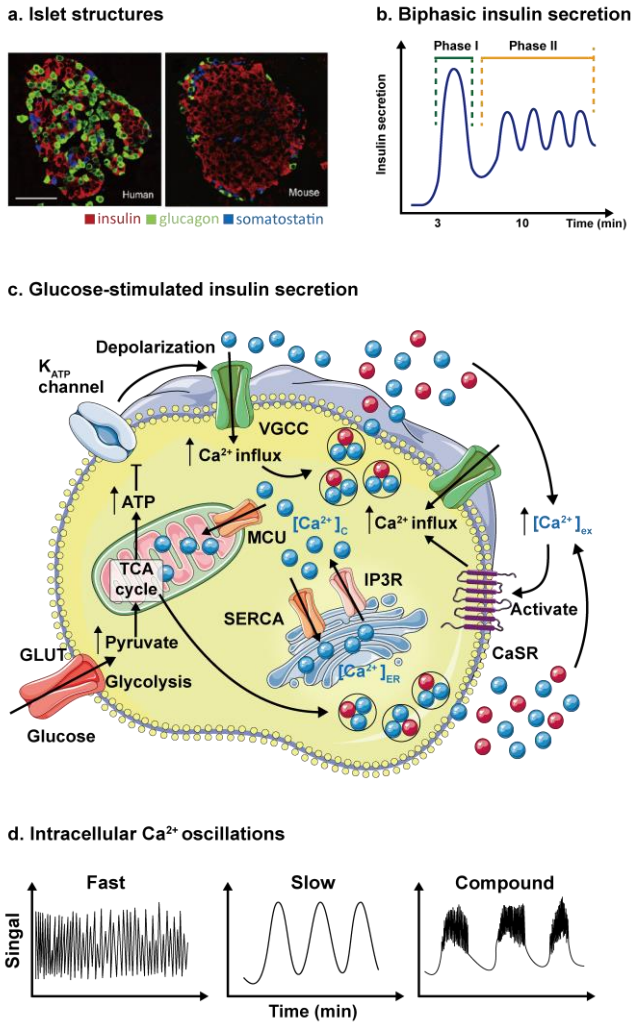

Figure 2 | Physiology of insulin secretion and Ca^{2+} signalling. a | Confocal fluorescence microscopy images of human and mouse pancreatic islets with immunostaining of insulin (red), glucagon (green) and somatostatin (blue). Scale bar, 50 μm. Reproduced with permission.[26b] Copyright 2013, Elsevier. **b |** Representative of biphasic insulin secretion of pancreatic islets, where a transient peak of insulin secretion is followed by a trail of oscillatory insulin release of smaller amplitude compared with the preceding phase; **c |** Schematics of Ca^{2+} signalling in the course of glucose-stimulated insulin secretion (GSIS). Subsequent to the rise of blood glucose and increased production of ATP in β cells, the closure of K_{ATP} channel reduces the hyperpolarizing K_{ATP} current and induces a depolarizing current, which leads to the opening of voltage-gated Ca^{2+} channel (VGCC) and the consequent influx of Ca^{2+}. The latter triggers the firing of action potential and the fusion of pre-existing insulin-containing granules with the membrane to release insulin, i.e. the phase I secretion. Meanwhile, the production of ATP promotes the synthesis of insulin in endoplasmic reticulum, which sustains the slow, oscillatory insulin release, i.e. the phase II secretion. During this biphasic secretion process, mitochondria and endoplasmic reticulum (ER) participate in the regulation of cytoplasmic Ca^{2+} concentration by storing (via MCU and SERCA) or discharging (via IP_3R) Ca^{2+}. Exocytosis of the secretory granules containing insulin and Ca^{2+} means that insulin and Ca^{2+} are co-released into the extracellular domain (exocytosis of granules containing other molecules is not discussed). The presence of Ca^{2+} in the extracellular domain may in turn activate the Ca^{2+}-sensing receptor to

signal VGCC for the Ca^{2+} influx. **d |** Three typical patterns of Ca^{2+} oscillation in cytoplasm during insulin secretion.

In both humans and rodents, the secretion of insulin is maintained at a low basal level during the fasting state, when blood glucose concentrations usually fluctuate between 3.9-5.6 mM in humans[27] and 3.4-7.2 mM in mice.[28] In response to elevated glucose levels (e.g. following intravenous glucose administration), insulin is released in a highly coordinated manner, comprising an early, rapid release (Phase I) and a later, slower, but sustained oscillatory release (Phase II) to facilitate glucose metabolism (Figure 2b).

In 1967, Anderson *et al* observed a pulsatile pattern of insulin concentrations in the portal vein of a dog 14 hours after meal ingestion.[29] Subsequent studies have revealed that insulin is secreted in an oscillatory manner from the islets.[30] The pulsatility of insulin secretory cycles has been reported to vary from 2 to 13 minutes, probably due to the differences in blood sampling sites (e.g., portal vs. peripheral vein) and frequencies between studies. However, the majority of studies reported 5-10 minutes per cycle.[31] That the oscillatory patterns of insulin secretion between the pancreas *in vivo* and individual islets *ex vivo* are almost identical, suggests that the secretion of insulin is synchronized between β cells both within an individual islet and across all stimulated islets in the pancreas.[32]

The amplitude of insulin pulses is diminished in patients with type 2 diabetes mellitus (T2DM), although the overall release of insulin may be augmented in the face of insulin resistance. In healthy individuals administered somatostatin-14 (which suppresses endogenous insulin secretion), administration of exogenous insulin in a pulsatile manner (a 2-minute infusion pulse every 11 minutes), compared to a constant infusion, was shown to be more effective at lowering blood glucose (mean blood glucose nadir 4.66±0.08 mM versus 5.53±0.06 mM).[33] In patients with type 1 diabetes mellitus (T1DM), the insulin requirement for suppressing hepatic glucose production is ~40% less when given in a pulsatile manner compared to continuous insulin

administration.[34] Accordingly, exposure to insulin in a pulsatile pattern appears critical to its glucose-lowering efficacy. The attenuated amplitude of insulin pulses observed in first-degree relatives of patients with T2DM may therefore represent an important deficit, predisposing them to T2DM.[35]

2.2 Intracellular Ca^{2+} signalling: a trigger for insulin secretion

Intracellular Ca^{2+} is an integral messenger that signals a cascade of intracellular activities of major relevance to the secretion of insulin. As depicted in Figure 2c, in response to elevated glucose, glycolysis driven by the enzyme phosphofructokinase-1 (PFK1) increases adenosine triphosphate (ATP), which gives rise to the closure of ATP-sensitive potassium channels (K_{ATP} channel) and hence cellular depolarization.[36] The latter is also accompanied by the opening of voltage-gated Ca^{2+} channels (VGCC, also known as voltage-dependent Ca^{2+} channel).[37] Due to the stark contrast in concentrations between $[Ca^{2+}]_{ex}$ (~1 mM) and $[Ca^{2+}]_c$ (100 nM), a burst of Ca^{2+} influx temporarily drives $[Ca^{2+}]_c$ up to 1 μM, triggering an action potential and fusion of insulin-containing granules with the cytoplasmic membrane to release insulin and other small molecules including Ca^{2+},[38] i.e. the exocytosis of insulin. This process is known as first-phase insulin secretion, associated with an abrupt peak during the first 10 minutes after stimulation (Figure 2b, Phase I). Elevated cytoplasmic Ca^{2+} (up to ~1 μM) is swiftly transported into the mitochondria (~100 μM $[Ca^{2+}]_{mito}$) and ER (~500 μM $[Ca^{2+}]_{ER}$) via the aforementioned transporters to allow $[Ca^{2+}]_c$ to return to the basal level. Concurrently, $[Ca^{2+}]_{mito}$ signals an enhanced synthesis of ATP to ensure energy supply for subsequent insulin synthesis.[39] As an intracellular reservoir of Ca^{2+}, the ER buffers intracellular Ca^{2+} and shapes the pattern of $[Ca^{2+}]_c$ oscillation during insulin release. The ER also accommodates the conversion of preproinsulin to proinsulin, which is subsequently folded and packaged into secretory granules,

together with proinsulin converting proteases and small molecules such as Ca^{2+} and Zn^{2+}.[40] Consequently, exocytosis of insulin granules is anticipated to increase $[Ca^{2+}]_{ex}$.[41] As long as the energy supply from glycolysis continues, synthesis, assembly and exocytosis of insulin can be sustained, forming the second phase of insulin secretion (Figure 2b, Phase II). These processes highlight (i) the intimate involvement of intracellular Ca^{2+} and (ii) the important role of Ca^{2+} oscillation in the respective domains.[42]

Several lines of observation support the importance of Ca^{2+} signalling pathways in glucose-stimulated insulin secretion (GSIS). Within the cytoplasm, oscillations of $[Ca^{2+}]_c$, with a typical periodicity of 5-10 minutes in both dispersed β cells[43] and coordinated β cells in intact islets,[44] coincide with those of insulin secretion, both of which are markedly suppressed once VGCC is blocked.[45] Oscillations of $[Ca^{2+}]_{mito}$ are in line with those of $[Ca^{2+}]_c$.[46] Silencing MCU[47] or retarding the change of $[Ca^{2+}]_{mito}$,[48] has therefore been found to attenuate the synthesis of ATP and second-phase insulin secretion. Similarly, $[Ca^{2+}]_{ER}$ increases following the rising $[Ca^{2+}]_c$ due to the influx of Ca^{2+} via SERCAs (including SERCA2b and SERCA3), and decreases in phase with the downstroke of $[Ca^{2+}]_c$ oscillation.[49] Manipulation of the activity of SERCAs thus affects the buffering effect of ER on $[Ca^{2+}]_c$. Indeed, the amplitude of glucose-induced $[Ca^{2+}]_c$ is augmented in SERCA3 knock-out β cells and by thapsigargin, which blocks all SERCAs.[50] Along with an enhanced amplitude of $[Ca^{2+}]_c$ oscillation, insulin secretion is also amplified.[50c, 51]

Hitherto, three patterns of $[Ca^{2+}]_c$ oscillation have been observed in β cells, including fast oscillation (small amplitude with periodicity at tens of seconds), slow oscillation (large amplitude with a cyclical pulse every 5-10 minutes) and compound oscillations (a hybrid pattern of fast superimposed on slow oscillations) (Figure 2d).[16] Given the match of the fast and slow frequency between insulin and $[Ca^{2+}]_c$, it is tempting to attribute the pulsatility of insulin secretion to the oscillation of $[Ca^{2+}]_c$. However, the role of other metabolic processes

in affecting the rate of insulin secretion should not be underestimated. For example, the M-type isoform of the glycolytic enzyme phosphofructokinase (PFK-M) is known to exhibit oscillatory activity with a similar periodicity as that of insulin.[52] In addition, the amplitude of pulsatile insulin release in the fasting state is impaired in humans with PFK-M deficiency.[53] Moreover, insulin secretion from pancreatic β cells can be decoupled from changes of $[Ca^{2+}]_c$ in MIN6 cells that are depolarized by 40 mM KCl.[54]

2.3 Intercellular Ca^{2+} signalling: an integrator for insulin secretion?

The coherent insulin secretory patterns between β cells within an individual islet, or stimulated islets within the pancreas, suggest that a fast signalling factor(s) instantaneously coordinates the activities within and between islets. Relative to neurotransmitters, intra-islet hormones and gut-derived incretin hormones, extracellular Ca^{2+} appears to be a dominant factor for synchronizing insulin secretion, via the Ca^{2+}-sensing receptor (CaSR), a G-protein-coupled receptor expressed abundantly on β cells.[10, 55]

As the name suggests, CaSR was initially discovered as a sensor for variations in $[Ca^{2+}]_{ex}$ in order to regulate the release of parathyroid hormone.[56] The following extensive investigations have revealed that CaSR signalling is essential to a variety of cellular processes, including differentiation[57] and apoptosis.[58] A study performed by De Luisi and Hofer has uncovered an important role of CaSR signalling in mediating intercellular communication. In that work, non-CaSR-expressing BHK-21 cells (donor cells) and CaSR-expressing HEK293 cells (HEK-CaSR, sensor cells) were co-cultured. Treatment with the Ca^{2+}-mobilizing agonist histamine (selective to BHK-21 cells) increased the $[Ca^{2+}]_c$ of BHK-21 cells and induced active extrusion of Ca^{2+} into the extracellular space. An increase in $[Ca^{2+}]_c$ was also observed in adjacent HEK-CaSR cells (<10 μm away) with a delay of fewer than 10 seconds, suggesting an activated intracellular signalling cascade in the HEK-CaSR. By contrast, the stimulated BHK-21 cells

failed to elicit the same change of $[Ca^{2+}]_c$ in wild type HEK293 cells. These observations provide strong support for the role of CaSR in intercellular communication.[59]

In the context of β cells (e.g. MIN6 cells), activation of CaSR over 48 hours using the calcimimetic R568 was reported to double the expression of epithelial-cadherin, indicating an increased cell proliferation. Moreover, CaSR activation increased L-type VGCC expression by 70% compared to control, leading to augmentation of the basal-to-peak amplitude of $[Ca^{2+}]_c$ in response to ATP and tolbutamide (both of which close potassium channels),[60] and increased insulin secretion, particularly in the presence of sufficient $[Ca^{2+}]_{ex}$ in the culturing medium.[61] Conversely, down-regulation of CaSR expression on MIN6 cells, even when cultured in islet-like three-dimensional architecture, was associated with a marked reduction in GSIS.[62]

Box 1 Intercellular communication via gap junctions or Ca^{2+}?

Gap junctions (Gjs) comprise specialized proteins/channels that physically connect adjacent cells and mediate rapid exchange of small molecules between them. Within the islets, Gjs are spatially restricted to adjacent β cells. However, the cellular network of the endocrine cells differs substantially between humans and rodents (Figure 2). Such a distinction in architecture argues against the role of Gjs as a universal integrator of coordinated insulin secretion.

Nevertheless, in mouse islets, Gjs facilitate the spreading of membrane depolarization and transmission of stimulatory signals between neighboring β cells by selectively transporting cations and small molecules.[42] Disruption of Gjs, to some extent, impairs $[Ca^{2+}]_c$ oscillation and normal GSIS. These observations suggest that the communication between β cells in mice relies, at least in part, on Gjs.[63]

3. Conventions of sensing cellular Ca^{2+} in islets

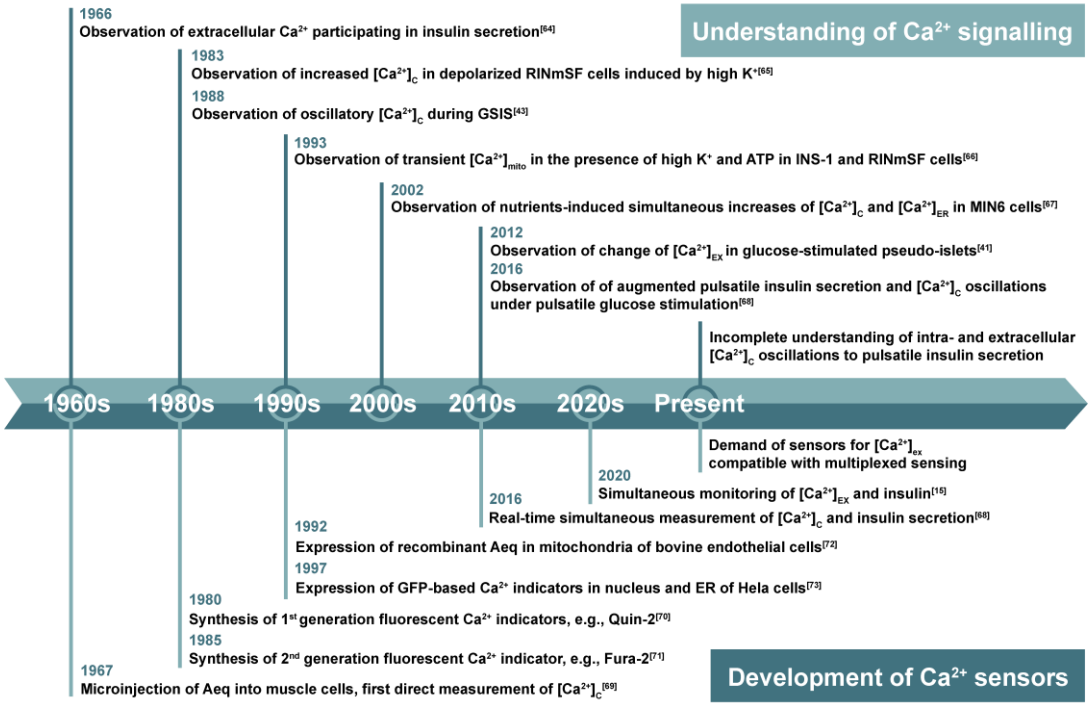

Figure 3 | Development of understanding of the role of Ca^{2+} in insulin secretion in relation to the evolution of Ca^{2+} sensing methods. While Quin-2 and Fura-2 have been prominent, there are serial relevant indicators invented and utilized over this timeframe. Our illustration focuses on concurrent measurements of Ca^{2+} and insulin, but there are many other key developments, e.g. the multiplexed sensing of $[Ca^{2+}]_c$ and the surrogate markers for insulin exocytosis (such as Zn^{2+}, which is co-released with insulin,[54] or phosphatidylinositol-3,4,5-trisphosphate (PIP3, which is coupled to the autocrine effect of insulin).[74] RINmSF: an insulin-releasing clonal cells.

Over the last six decades, the development of sensing methodologies has underpinned major knowledge gains in relation to cell biology. The invention of Ca^{2+} sensors and associated techniques/platforms has, in particular, played an indispensable role in the understanding of the secretory function of pancreatic β cells and islets, as illustrated in **Figure 3**.

In 1966, omission of Ca^{2+} but not Mg^{2+} in the perfusate was found to inhibit insulin secretion from isolated rat pancreas *in vitro*, highlighting that extracellular Ca^{2+} is a prerequisite for insulin secretion.[64] In the next year, the discovery and application of the luminescent protein,

aequorin (Aeq), isolated from the *Aequorea* jellyfish, made it possible to record intracellular Ca^{2+} (i.e., $[Ca^{2+}]_c$) for the first time in living cells.[69] Aeq and its derivatives were popular tools for Ca^{2+} sensing over the subsequent 20 years, but failed to enrich understanding of physiology substantially due to their intrinsic limitations, including low fluorescence and the need for continuous replacement of oxidized components. This stagnation emphasizes the importance and urgency of developing Ca^{2+} indicators with bright fluorescence and high sensitivity to changes of $[Ca^{2+}]$. Moreover, the upcoming indicators should be introduced into cells in a manner less invasive than microinjection, which was used for Aeq. In the 1980s, the synthetic Ca^{2+} indicators (e.g. Quin-2[70] and Fura-2[71] of stronger fluorescence than Aeq) were developed, and their applications in β cells revealed the oscillations of $[Ca^{2+}]_c$ during the GSIS.[43, 75] Conjugation of the membrane-permeable acetoxymethyl (AM) ester with the synthetic indicators also enabled non-invasive loading of the Ca^{2+} indicators into cytoplasm.[76] Between 1990-2000s, with the advent and maturation of genetic editing and transcriptional regulation techniques, the expression of genetically encoded Ca^{2+} indicators (GECIs), including recombinant Aeq[73] and fluorescent proteins (FPs)-based Ca^{2+} indicator[73], into a specific subcellular compartment of living cells was established. The applications of these GECIs on monitoring Ca^{2+} dynamics in the organelles of β cells has revealed links between insulin secretion and Ca^{2+} oscillations in the mitochondria (in 1993)[66] and ER (in 2002).[67] Complementary to the measurement of intracellular Ca^{2+}, Ca^{2+}-selective microelectrodes (CSMs) have advanced the monitoring of $[Ca^{2+}]_{ex}$ in the vicinity of β cells[77] and in the extracellular cavity within a pseudo-islet, such as that formed by INS-1E cells.[41] In these models, the elevation of glucose levels is found to induce substantial fluctuations of $[Ca^{2+}]_{ex}$ in the interstitial space around β cells, providing the basis for an autocrine/paracrine cell-to-cell communication via $[Ca^{2+}]_{ex}$. However, the point-of-care measurement by CSMs is insufficient to elucidate whether and how such intercellular communication functions in the scale of intact

islets. Therefore, novel Ca^{2+} sensors are needed to comprehend the roles of $[Ca^{2+}]_{ex}$ in modulating and synchronizing insulin secretion.

Box 2 Considerations of choosing Ca^{2+} indicators in practice

Dissociation constant (K_d)

K_d is a fundamental parameter of an indicator, which is used to measure the propensity of its binding to the target (i.e., Ca^{2+} in the current context).[78] At the equilibrium, K_d, in relation to the binding kinetics between Ca^{2+}, the indicator (noted as *N*), and their complex molecule (noted as *CaN*), is expressed as follow:

$$K_d = \frac{[Ca^{2+}] \times [N]}{[CaN]}$$

The equilibrium concentration of Ca^{2+} can be calculated by:

$$[Ca^{2+}] = K_d \left(\frac{F - F_{min}}{F_{max} - F}\right)$$

where *F* is the fluorescence of Ca^{2+}-bound indicator, F_{min} is the background fluorescence in the absence of Ca^{2+} and F_{max} is the fluorescence when all indicator molecules are bound to Ca^{2+}.

Based on the law of mass action, $0.1–10 \times K_d$ defines the indicator's effective sensing range, representing the scope of approximately 20–80% of the indicators bound to Ca^{2+}, over which fluorescence intensity changes linearly as a function of $[Ca^{2+}]$ on a logarithmic scale.[24a] To accurately quantify $[Ca^{2+}]$ and its variations at different cellular compartments, the K_d of an indicator needs to be taken into account in the search of the most appropriate indicator(s). For instance, Fura-2, with K_d at 224 nM, is suitable to track intracellular $[Ca^{2+}]$, but not extracellular $[Ca^{2+}]$, since the latter approximates 1 mM (exceeding 10 times of its K_d). Similarly, it is suboptimal to use Quin-2 (K_d, 60 nM) to monitor glucose-induced oscillations

of $[Ca^{2+}]_c$ with amplitudes as high as 1000 nM (Figure 1a), beyond the upper limit of the indicator (600 nM).[79]

Intensity-based or ratiometric indicator?

In general, it is challenging to employ an intensity-based indicator for quantitative analysis of Ca^{2+}, partly because the signal of an indicator is prone to self-shifting as a function of its concentration, thereby interfering with precise quantification of $[Ca^{2+}]$.[80] Other factors, including its heterogeneous distribution, leakage and photobleaching as well as non-uniform excitation conditions, further confound efforts to evaluate $[Ca^{2+}]$ quantitatively.

In contrast, a ratiometric indicator has the potential to circumvent the aforementioned limitations since, by definition, it relies on ratios of the signal at different wavelengths, i.e. relative intensity, so is intrinsically self-calibrated.

3.1 Chemically synthesized fluorescent indicators for $[Ca^{2+}]_c$

The jellyfish-sourced luminescent protein Aeq, emitting blue luminescence spontaneously after binding to Ca^{2+}, was once a spearhead for sensing Ca^{2+}. Its weak fluorescence, however, has become a major obstacle to its utility for tracing Ca^{2+} in biological studies. Therefore, many other indicators have been developed; some examples are listed in **Table 1**. Unless otherwise specified, Ca^{2+} indicators discussed in this section predominantly refer to those used in islet studies.

Chemically synthesized fluorescent indicators are the most widely used cellular Ca^{2+} sensors. They usually consist of a fluorophore, Ca^{2+} chelator (such as 1,2-bis(*o*-aminophenoxy)-ethane-*N*, *N*, *N*′, *N*′-tetraacetic acid (BAPTA)), and a linker. The binding affinity of such an indicator to Ca^{2+} depends on the property of the Ca^{2+} chelator and its intramolecular electronic state after conjugation with the fluorophore and linker. The dissociation constant (K_d) describes the

propensity of an indicator to bind Ca^{2+} and, hence, defines the effective sensing range. Accordingly, K_d should be the first key consideration when assessing the suitability of a synthetic Ca^{2+} indicator (Box 2). Another consideration relates to the alternations of the optical property of the indicator upon binding to Ca^{2+}, including the variation in the intensity of fluorescence and the shift in the peak of excitation/emission wavelengths (Box 2). Moreover, the fluorescence signals may vary substantially because of the specific experimental setup for Ca^{2+} imaging/sensing, including the use of excitation light and filters as well as the configuration of the photodetector.

There are three principal mechanisms underlying Ca^{2+}-induced optical changes for chemically synthesized fluorescent Ca^{2+} indicators and GECIs, including photo-induced electron transfer (PiET), internal charge transfer (ICT) and Förster resonance energy transfer (FRET).[81]

Table 1. Chemically synthesized indicators for sensing $[Ca^{2+}]_c$

Indicators	K_d (nM)	Excitation nm		Emission nm		F_{max}/F_{min} (R_{max}/R_{min})	Subjects	Note	Ref.
		Ca^{2+} free	Ca^{2+} bound	Ca^{2+} free	Ca^{2+} bound				
Quin-2	60	355	330	495	495	5-8	1, 6	a	[65, 82]
Fura-2	224	380	340	510	505	(13-25)	1, 2, 3, 4	b	[83]
Indo-1	230	346	330	475	400	(20-80)	2	c	[44a]
Fura-PE3	250	364	334	508	500	(18)	2	d	[50c, 84]
Fluo-3	390	503	506	525	525	40-100	4	e	[44b]
Fura-red	140	470	435	660	660	(5-12)	2, 4, 5	f	[74, 85]

Note: F_{max}/F_{min}, ratio of maximum to minimum of fluorescence of indicator; R_{max}/R_{min} contrast of ratios of maximum fluorescence to minimum fluorescence between Ca^{2+}-free and Ca^{2+} bound states of indicator. Besides the listed references, we also refer to *The Handbook: A Guide to Fluorescent Probes and Labelling Technologies* (11 ed.).[86] F_{max}/F_{min} or R_{max}/R_{min} is provided depending on which is available.

Subjects:

1. Isolated mouse β cells
2. Intact mouse islet
3. Isolated human β cells
4. Intact human islet
5. MIN6 β cells (highly differentiated and glucose-responsive murine β cell line)[87]
6. Clonal insulin-releasing cell line RINm5F

Note:

a. The first generation indicator, whose absorption and quantum efficiency are lower than fluorescent indicators developed subsequently.[24a]
b. A ratiometric indicator featuring high compartmentalization and strong protein binding characteristics.
c. A ratiometric indicator with dual emissions.[44a]
d. A Fura-2 derivative developed for monitoring leakage resistance of cytoplasmic Ca^{2+} (i.e., the efflux process). The absorption peak of Fura-PE3 undergoes a significant blue shift upon binding Ca^{2+}.
e. An indicator featuring enhanced fluorescence and visible excitation light (thus, reduced photodamage).
f. A ratiometric indicator, characteristic of a long-wavelength emission, such as red, and used for multiplexing sensing in conjunction with other ion-sensitive indicators.

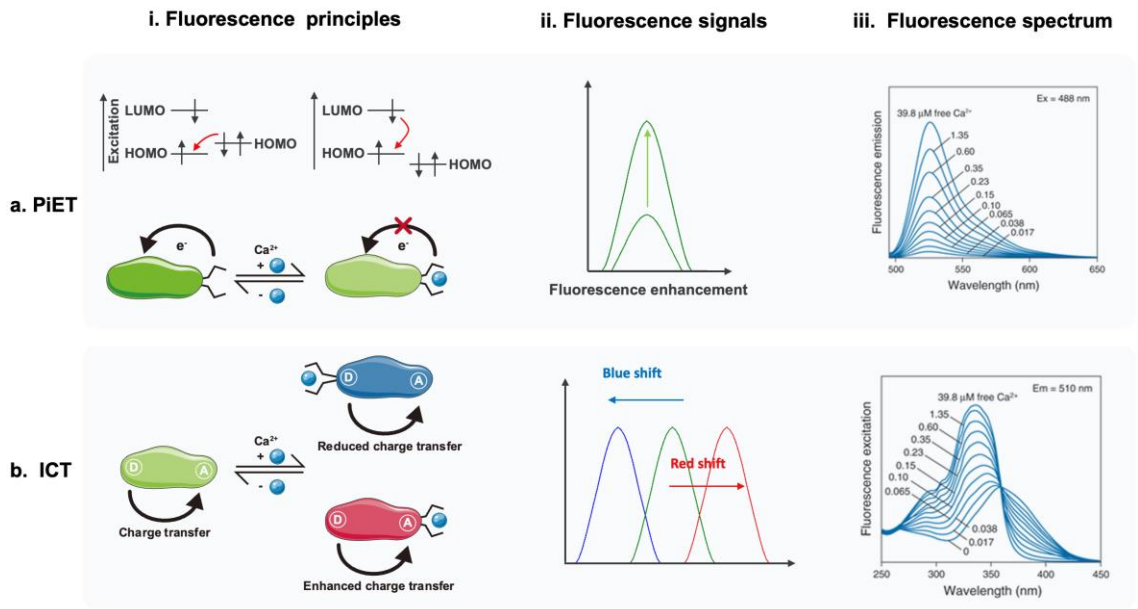

Figure 4 | Schematic of fluorescent principles and optical responses of chemically synthesized fluorescent indicators upon binding Ca^{2+}. a | Photo-induced electron transfer (PiET)-based fluorescent indicator: **i |** Energy scheme and reversible process of binding/unbinding Ca^{2+} in the regulation of the optical responses; **ii |** Fluorescence enhancement of PiET-based indicator in the presence of Ca^{2+}, where a spectral shift is usually negligible even if it occurs; **iii |** Fluorescence enhancement of PiET-based Fluo-3 proportional to increase in [Ca^{2+}] (excitation 488nm, emission ~525 nm). Reproduced with permission.[86] Copyright 2011, Springer Nature. **b |** Internal charge transfer (ICT)-based fluorescent indicators: **i |** Schematic of Ca^{2+}-modulated ICT process. In the absence of Ca^{2+}, ICT occurs as the charge transfer from the electron donor (denoted by D, e.g. dialkylamino-) to the electron acceptor (denoted by A, e.g. carbonyl). When a Ca^{2+} chelator is linked to D (negatively charged), binding of Ca^{2+} suppresses the electron transfer from D to A (blue); on the contrary, Ca^{2+}-binding with the chelator linked to A enhances the ICT (red); **ii |** A reduced ICT leads to a blue shift of the emission band, while an enhanced ICT undergoes a red shift; **iii |** Shift of

excitation spectra of Fura-2 (an ICT-based fluorescent indicator) in response to Ca^{2+}. Reproduced with permission.[86] Copyright 2011, Springer Nature.

As shown in **Figure 4a, i** (left), for a PiET-based indicator, electrons of the fluorophore on the highest occupied molecular orbital (HOMO) are re-populated to its lowest unoccupied molecular orbital (LUMO) upon light excitation.[88] The consequent electron vacancies in the HOMO of the fluorophore are inclined to be re-filled by its intrinsic electrons on LUMO via radiative de-excitation. At the same time, the electrons on the HOMO of the chelator compete to fill the vacancies, which prohibits the relaxation of the fluorophore and the subsequent fluorescence emission. In the case of binding between chelator and Ca^{2+} (Figure 4a, i (right)), the chelator experiences an increase in redox potential, pulling its HOMO energy level below the HOMO of fluorophore, so that electron transfer from chelator to fluorophore is effectively suppressed. As a result, radiative relaxation of excited electrons on the fluorophore LUMO becomes dominant, producing emission of an unquenched fluorescence. Such a fluorescence response in the absence/presence of Ca^{2+} is depicted in Figure 4a, ii. Since the degree of impedance of the competitive de-excitation channel is sensitive to the availability of Ca^{2+} to the indicators (i.e., the concentration of Ca^{2+}), its fluorescence behavior is $[Ca^{2+}]$-dependent (Figure 4a, iii).[24e] The indicator maintains its sensitivity to the changes of $[Ca^{2+}]$ as long as Ca^{2+}-binding sites of the chelators are not saturated.

ICT-based indicators are constructed by a pair of so-called donor and acceptor molecules that occupy each end of a fluorophore via a direct conjugation (Figure 4b, i). Both the donor and acceptor possess Ca^{2+}-binding sites (without a linker). Upon light excitation, the electron transfer from the donor to acceptor is accompanied by an instantaneous change in the dipole moment of the fluorophore. The relaxation of the dipole leads to a Stoke-shifted fluorescence of the fluorophore. The flexibility of anchoring the chelator onto either the donor (D) or acceptor (A) side allows ICT-based indicators to exhibit blue- or red-shift fluorescence (Figure

4b, ii).[89] A blue shift occurs when both the electron-donating property and conjugation strength of the donor are restrained by the chelator; conversely, a red shift appears when the electron-withdrawing property of the acceptor is enhanced by the adjacent chelator.[90] Fura-2 is a representative ICT-based fluorescent indicator. As shown in Figure 4b, iii, the excitation spectrum peak of Fura-2 shifts from ~380 to ~340 nm with increasing fluorescence intensity in response to the increased binding of Ca^{2+} to its donor side. In addition, the ratiometric feature of Fura-2 at 340/380 nm offers self-calibrated fluorescence signals and hence minimizes the potential interference from the sensing environment. In this context, a ratiometric indicator may be preferable to an intensity-based indicator for quantification of [Ca^{2+}] (Box 2).

Despite tremendous successes in probing intracellular Ca^{2+}, the advent and development of chemically synthesized fluorescent Ca^{2+} indicators have faced several issues. First, photobleaching, a notorious problem with almost all these indicators, interferes with precise quantification of [Ca^{2+}] during long-term tracking, resulting in limited observation window.[91] Second, exposure to UV light is associated with phototoxicity, which impairs cellular function. Substitution for the visible light-excitable indicators seems to be a rational option to circumvent photobleaching and reduce phototoxicity. However, only a few Ca^{2+} indicators that are excitable by visible light have been developed, providing a limited range of K_d and optical performance. In light of these limitations, the use of ratiometric indicators appears preferable in principle.[92] However, interferences caused by compartmentalization, leakage and incomplete hydrolysis may still disrupt the recording or interpretation of results.[24a]

3.2 Genetically encoded Ca^{2+} indicators for $[Ca^{2+}]_c$

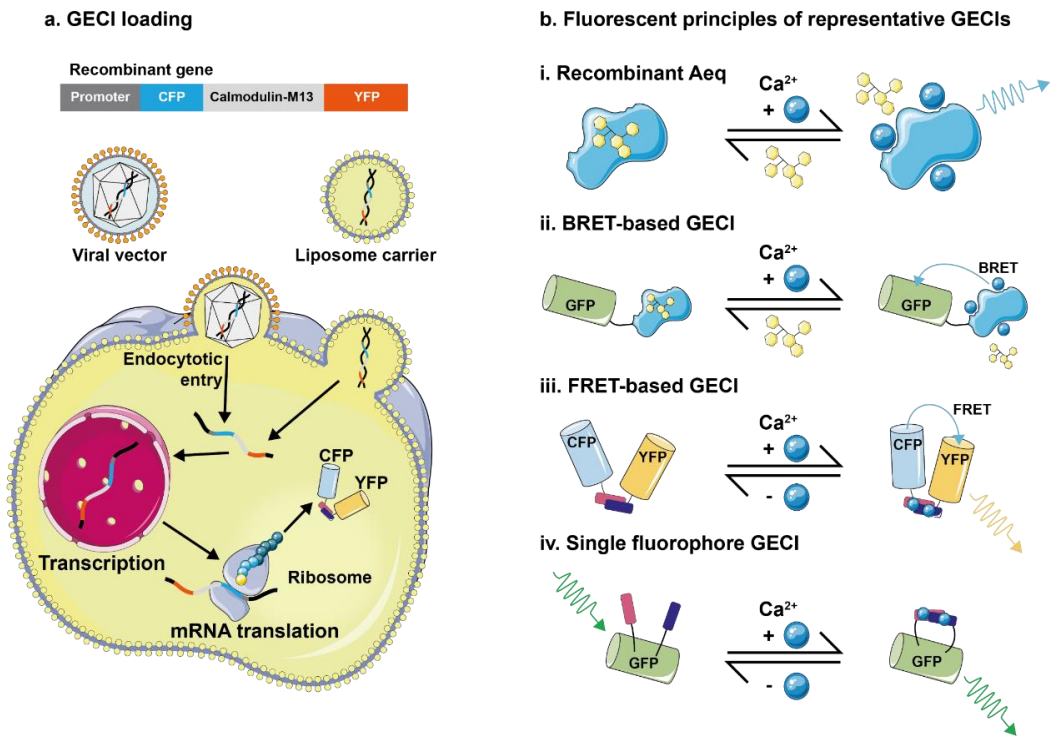

Figure 5 | Transfection and sensing principles of representative GECIs. a | Schematic of viral transfection or lipofection loading of GECIs into a target cell. The viral vector or liposome carrier embedded with the fusion recombinant gene transfects the host cell by releasing the fused DNA. The indicator DNA is added into the host gene by integrase and subsequently expressed in the target compartment after DNA transcription and mRNA translation; **b |** Fluorescence principles of representative GECIs. **i |** In the presence of Ca^{2+}, recombinant Aeq, undergoing internal oxidation of coelenterazine to coelenteramide, releases a coelenteramide and gives emission at 470 nm. Its reversible pathway - refunctionalization of Aeq - proceeds with the provision of coelenterazine; **ii |** Bioluminescence resonance energy transfer (BRET)-based GECI comprises a single green fluorescent protein (GFP) and its conjugated Aeq, showing GFP's fluorescence once Ca^{2+} binding switches on the emission of Aeq since the latter overlaps with the absorption of Aeq; **iii |** A representative of Förster resonance energy transfer (FRET)-based GECI, typically consisting of a cyan fluorescent protein (CFP), a yellow fluorescent protein (YFP), a Ca^{2+}-binding peptide calmodulin (CaM, linker in black) and a CaM-binding peptide M13 (linker in red). Conformational changes of CaM and M13 induced by binding Ca^{2+} lead to a reduced distance between CFP and YFP. Under external light excitation, the shortened distance between CFP and YFP accelerates the FRET, i.e., a portion of fluorescence of CFP will be absorbed by YFP for its own emission; **iv |** Single fluorophore-based GECI, for example, a GFP conjugated with CaM and M13. The binding of Ca^{2+} induces conformational changes to both CaM and M13, hence modulating the optical properties of the GFP.

GECIs, also known as fluorescent Ca^{2+} indicator proteins (FCIPs), are another mainstay optical toolkit for sensing $[Ca^{2+}]_c$. As described in **Figure 5a**, the nucleic acid sequence of the indicator is tagged with a selected promoter sequence from the target organelle. The fused cDNA is then

transfected into the target cells, mostly via lipofection[72] or viral transduction.[93] Under the guidance of a promoter gene, GECIs can be precisely expressed in the target subcellular compartment, e.g., mitochondria, ER, nucleus, Golgi and plasma membrane. Similar to chemically synthesized indicators, the optical property (mostly the fluorescence intensity) of GECIs is altered upon binding Ca^{2+}. For the selection of a suitable GECI, both K_d and the optical property remain key considerations.

As shown in Figure 5b, four types of GECIs are widely used:

(i) **Recombinant Aeq** is a type of protein that is produced by reconstructing the native Aeq sequence using genetic engineering techniques. This can be achieved by transfecting cells with Aeq cDNA fused with a tag sequence for targeted expression.[94] Similar to the native Aeq, the recombinant Aeq expressed in cells exhibits spontaneous fluorescence at 470 nm when binding to Ca^{2+}.[72] The emission of fluorescence is accompanied by the oxidation of coelenterazine to colenteramide in the recombinant Aeq molecule (Figure 5b). Recombinant Aeq used in islet studies has allowed recording of the $[Ca^{2+}]_{mito}$, showing that $[Ca^{2+}]_{mito}$ increased and oscillated in MIN6 cells treated by KCl (22 mM) or glucose (30 mM) with a higher peak concentration than that of $[Ca^{2+}]_c$ (2 μM $[Ca^{2+}]_{mito}$ vs. 900 nM $[Ca^{2+}]_c$);[95] KCl-evoked elevation in $[Ca^{2+}]_{mito}$ induced an immediate increase in cytosolic and mitochondrial free ATP, suggesting that the $[Ca^{2+}]_{mito}$ is essential for mitochondrial metabolism, i.e., the production of ATP.[46b]

(ii) **Bioluminescence resonance energy transfer** (**BRET)-based GECI**, also called hybrid recombinant Aeq, is composed of a recombinant Aeq and a fluorescent protein, in which the excitation spectrum of the fluorescent protein is overlapped with the emission of Aeq, hence leading to BRET. As shown in Figure 5b, ii, as Ca^{2+} binding induces a conformational change to the indicator, the distance between Aeq and the fluorescent protein reduces, and then the BRET takes place and is stoked. As a result, the fluorescent protein is excited by the

luminescence of Aeq without the need for an external light source.[96] While BRET-based GECIs have improved the intensity of fluorescence signal compared with pure Aeq, their application in islet studies is limited by the demand of constant replacement of the oxidized component, i.e., the coelenterazine.

(iii) **FRET-based GECI** is constructed by connecting two FPs with a linker, e.g., Ca^{2+}-binding protein calmodulin and calmodulin-binding protein M13. The most frequently used FPs belong to the chameleon family. As shown in Figure 5b, iii, an exemplified FRET-based GECI is constituted by the cyan fluorescent protein (CFP) and the yellow fluorescent protein (YFP). In the absence of Ca^{2+}, the emission of CFP at 480 nm dominates. Upon binding to Ca^{2+}, an intramolecular conformational change occurs and pulls the two FPs closer, causing an enhanced FRET. As a consequence, YFP is switched on by the emission of CFP and emits fluorescence at around 530 nm.[73] In islet studies, for example, its use (e.g., Ycam-4ER, K_d = 100-1000 μM, and D4ER, K_d = 65 μM)[73, 97] has enabled the direct measurement of $[Ca^{2+}]_{ER}$ in response to varying stimuli and provided insights into the roles of Ca^{2+} transporters in the organelles of β cells. In particular, $[Ca^{2+}]_{ER}$ imaging using Ycam-4ER showed that $[Ca^{2+}]_{ER}$ increased in MIN6 cells with 20 mM glucose treatment. In addition, resting $[Ca^{2+}]_{ER}$ was markedly reduced after the suppression of SERCA2b but not SERCA3, suggesting that SERCA2b is the principal ER Ca^{2+}-ATPase in MIN6 cells.[67] Simultaneous monitoring of $[Ca^{2+}]_c$ and $[Ca^{2+}]_{ER}$, using Fura-PE3 and D4ER, respectively, revealed that $[Ca^{2+}]_{ER}$ oscillated concurrently with $[Ca^{2+}]_c$ under glucose stimulation. This study also demonstrated that the increase in $[Ca^{2+}]_{ER}$ was not abolished but only slightly decreased when SERCA3 was knocked out, reflecting the predominant role of SERCA2a in the regulation of $[Ca^{2+}]_{ER}$ within β cells.[51, 67]

(iv) **Single fluorophore GECI**, as a GCaMP family member, can be represented by indicators containing a circularly permuted GFP, conjugated with the Ca^{2+}-binding protein calmodulin on

one side and M13 on the other side.[98] Conformational changes in calmodulin induced by the presence of Ca^{2+} increase the interaction between calmodulin and M13, which in turn impacts the intramolecular protonation state of the fluorophore GFP. As such GFP fluorophore gives rise to enhanced emissions in proportion to the concentration of Ca^{2+} (Figure 5b, iv).[99] One selected example is the derivative of Pericam, 2mt8PR (K_d = 1.7 μM), which was invented for targeted expression in mitochondria of living cells.[100] The application of 2mt8PR in mouse β cells showed that the increase in $[Ca^{2+}]_{mito}$ induced by 17 mM glucose followed the elevated $[Ca^{2+}]_c$ with a temporal delay for around 80 seconds. In the same study, the increase in $[Ca^{2+}]_{mito}$ was substantially impaired when the expression of mitochondrial Ca^{2+} uniporter (MCU) was suppressed using shRNA. However, the fact that the increase in $[Ca^{2+}]_c$ was not affected by MCU silencing suggested an alternative pathway for clearing increased $[Ca^{2+}]_c$ in mouse β cells.[46a]

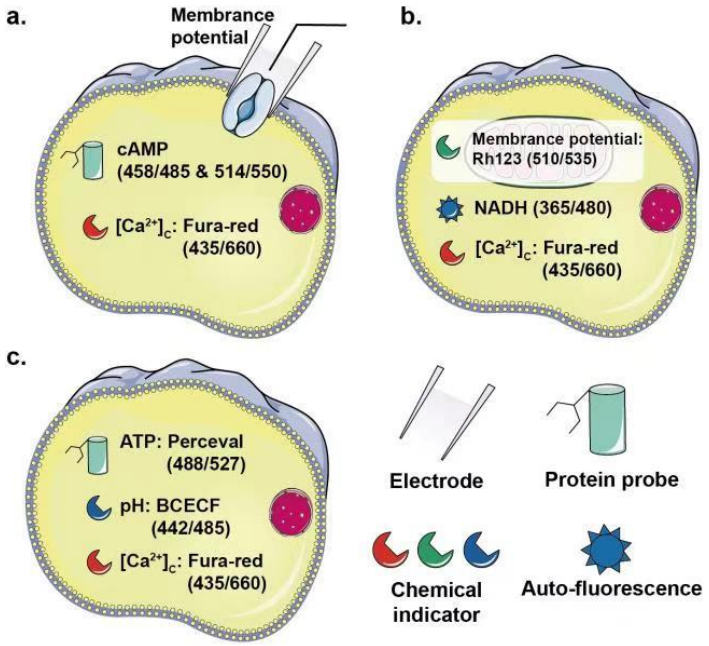

Figure 6 | Illustration of multiplexed sensing of $[Ca^{2+}]_c$, where simultaneous sensing is enabled by using long-wavelength emission of Fura-red ($\lambda_{ex}/\lambda_{ex}$: 435/660 nm) in combination with sensors for other concerned intracellular molecules, including: **a** | sensing of $[Ca^{2+}]_c$ by

Fura-red, cyclic adenosine monophosphate (cAMP) by a cAMP biosensor ($\lambda_{ex}/\lambda_{ex}$: 485/535 nm) and cytoplasmic membrane potential by patch-clamp;[74, 101] **b |** sensing of $[Ca^{2+}]_c$ by Fura-red, NADH by autofluorescence ($\lambda_{ex}/\lambda_{ex}$: 365/480 nm) and mitochondrial membrane potential by Rh123 ($\lambda_{ex}/\lambda_{ex}$: 510/535 nm);[85a] **c |** sensing of $[Ca^{2+}]_c$ by Fura-red, ATP by Perceval ($\lambda_{ex}/\lambda_{ex}$: 488/527 nm) and pH by BCECF ($\lambda_{ex}/\lambda_{ex}$: 442/485 nm).[85b]

Clarifying the complex interaction of multiple biofactors that constitute the signalling network underlying insulin secretion is critical to the understanding of the islet biology. For this purpose, multiplexed sensing, deploying multiple sensors for concurrent monitoring of $[Ca^{2+}]_c$ and other regulatory factors, is of importance. For example, cyclic adenosine monophosphate (cAMP) is an intermediate regulator that has been considered to enhance intracellular Ca^{2+} signal and exocytosis via protein kinase A (PKA)-dependent and -independent pathways. While cAMP signalling is pivotal to the insulinotropic effect of gut hormones, the correlation between intracellular cAMP and $[Ca^{2+}]_c$ was unclear. Simultaneous monitoring of $[Ca^{2+}]_c$ and cAMP has identified that cytoplasmic cAMP oscillates in β cells or MIN6 cells with the provision of 11 mM glucose. The pattern of cAMP oscillation resembled $[Ca^{2}]_c$ and partially relied on $[Ca^{2+}]_c$ oscillation, as inhibition of the $[Ca^{2+}]_c$ change using the VGCC blocker methoxyverapamil (50 μM) did not abolish cAMP oscillation. Therefore, the multiplexed sensing of $[Ca^{2+}]_c$ and cAMP has clarified that cAMP, while oscillating with $[Ca^{2+}]_c$, is not directly driven by the latter.[74] This enlightening work has stimulated further studies, which, for example, found that the suppression of cAMP formation by inhibiting adenylyl cyclase (the enzyme that converts ATP to cAMP) reduced GSIS from β cells, and that the effect of cAMP on modulating pulsatile insulin secretion could be mediated by a cAMP-dependent guanine nucleotide exchange factor, Epac2. Together, these observations have provided a novel understanding of the formation of pulsatile insulin secretion (**Figure 6a**).[74, 101]

Knowledge about the interaction between $[Ca^{2+}]_c$ and mitochondrial activity in β cells has also been advanced with the aid of multiplexed sensing methodology. Simultaneous measurements

of NADH (by autofluorescence), $[Ca^{2+}]_c$ (by Fura-red) and mitochondrial membrane potential (by Rh123) in mouse β cells under 10 mM glucose have shown that: (i) NADH oscillates around every 5 minutes; (ii) these oscillations are almost coherent with those of $[Ca^{2+}]_c$; (iii) $[Ca^{2+}]_c$ and NAD(P)H oscillations are both abolished with inhibition of L-type VGCC by nifedipine; and (iv) the effect of $[Ca^{2+}]_c$ is dependent on glucose, as elevated $[Ca^{2+}]_c$ augmented NADH autofluorescence of β cells at 3 mM glucose but lowered NADH autofluorescence at 10 mM glucose. These observations suggest that slow oscillations of NADH within intact islets are modulated by $[Ca^{2+}]_c$, such that intracellular Ca^{2+} represents a key element of feedback regulation of the respiratory activity in mitochondria (Figure 6b).[85a] Another illustration of multiplexed sensing relates to the simultaneous recording of $[Ca^{2+}]_c$ (by Fura-red) and cytoplasmic ATP concentrations (by Perceval, a protein-based ATP indicator) (Figure 6c), which has revealed that glucose induces pronounced oscillations of intracellular ATP, whose concentration is negatively correlated with $[Ca^{2+}]_c$. Of note, ATP oscillations were abolished once L-type Ca^{2+} channels were blocked by methoxyverapamil.

3.3 Ca^{2+}-selective microelectrode (CSM) for $[Ca^{2+}]_{ex}$

A CSM, generally comprising an amplifier, a voltmeter and sensing and reference electrodes, is made by combining an ion-selective functionality with a microelectrode (capable of measuring, for example, cell membrane potential, resistance and net ion transport). CSMs have been developed to trace concentration changes of a specific ion, such as Ca^{2+}, Na^+, K^+, H^+ and Cl^-.[102]

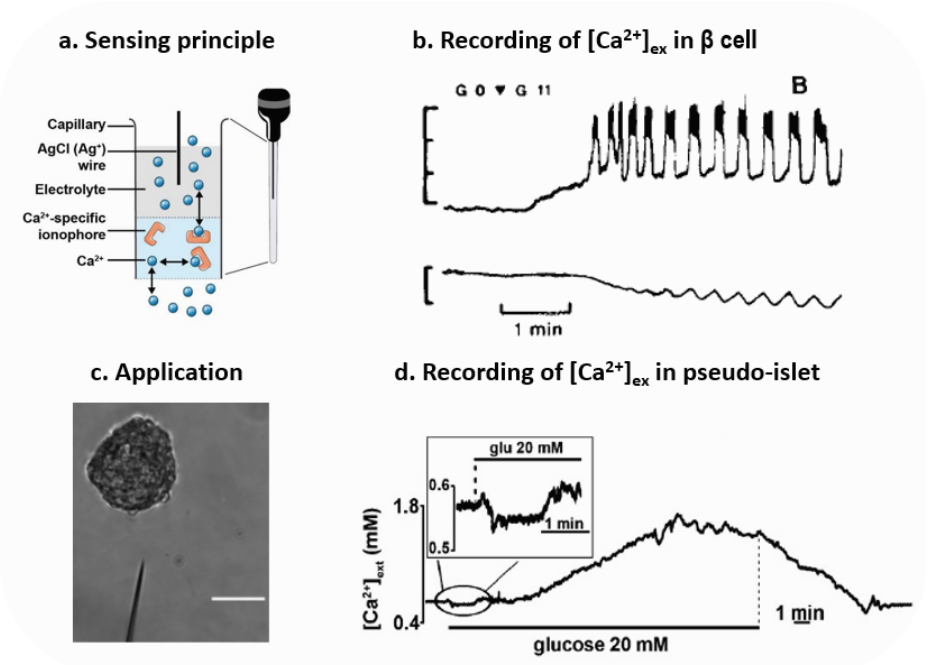

Figure 7 | Applications of a Ca^{2+}-selective microelectrode (CSM) in islet studies. a | Schematic of a CSM tip in measuring Ca^{2+}, where Ca^{2+}-selective ionophores can transport Ca^{2+} reversibly between the sample and the inner electrolyte. **b |** CSM measuring $[Ca^{2+}]_{ex}$ in combination with potential electrode measuring plasma membrane potential. Upper panel: Variations in β cell membrane potential upon increasing glucose from 0 to 11 mM; lower panel: corresponding changes of $[Ca^{2+}]_{ex}$ during this process. Reproduced with permission.[77] Copyright 1995, Elsevier. **c |** Microscope image illustrates the placement of a double-barrelled selective microelectrode in proximity to an INS-1E pseudo-islet. Scale bar, 100μm. Reproduced with permission.[41] Copyright 2012, Elsevier. **d |** Response of extracellular $[Ca^{2+}]$ of the pseudo-islet under stimulation with 20 mM glucose, measured by CSM inserted in the intercellular space. Reproduced with permission.[41] Copyright 2012, Elsevier.

Figure 7a is a schematic of a typical Ca^{2+} sensing electrode, which consists of a Ca^{2+}-selective ionophore cocktail (lipophilic liquid phase with ion-exchange properties), electrolyte (usually concentrated KCl solution containing Ca^{2+}), and a reference electrode (containing Ca^{2+}-free electrolyte).[103] Once there is a $[Ca^{2+}]$ difference between sample and internal electrolyte, Ca^{2+}-selective ionophores specifically bind Ca^{2+} and transport the Ca^{2+} between the sample and electrolyte, towards a concentration equilibrium. Alongside the transportation of Ca^{2+}, changes in the electric potential are induced between the microelectrode and the reference electrode, and the corresponding voltage is recorded by the voltmeter. Since the varying potential is proportional to the logarithm of $[Ca^{2+}]$ (based on the Nernst equation), CSMs will extract the dynamic changes of $[Ca^{2+}]$ accordingly.[104]

Perez-Armendariz and Atwater have made a pioneering contribution by exploiting CSMs to probe $[Ca^{2+}]_{ex}$ in the intercellular space of β cells.[105] They observed that, in a measurement lasting for ~1 minute, there is an instant depletion of 0.5 mM $[Ca^{2+}]_{ex}$ under glucose stimulation (11 mM), before reverting to the basal level. This observation has clarified that there is a correlation between the fast oscillatory $[Ca^{2+}]_{ex}$ and stimulation of the islet by glucose. Moura combined CSM (placed in the vicinity of the cell) with a potential-sensitive microelectrode (impaled within the β cell) for multiplexed sensing of $[Ca^{2+}]_{ex}$ and membrane electrical activity. This work showed that the addition of glucose (11 mM) depolarized the β cells and induced biphasic electrical activity accompanied by small oscillations of $[Ca^{2+}]_{ex}$ in an islet (Figure 7b). The respective waveforms of $[Ca^{2+}]_{ex}$ and membrane potential were essentially concomitant, with a delay of only 1 minute between the oscillatory behavior of $[Ca^{2+}]_{ex}$ and the membrane potential. These outcomes are in good agreement with the Ca^{2+} signalling process, i.e., membrane depolarization first induces Ca^{2+} influx from the extracellular space, followed by the transport of Ca^{2+} into the extracellular space during repolarization.[77] Gerbino *et al*. measured $[Ca^{2+}]_{ex}$ in the intercellular cavity by placing a CSM close to an INS-1E pseudo-islet (Figure 7c). They found that exposure of the pseudo-islet to both high glucose (20 mM) and non-nutrient insulinotropic compounds raised $[Ca^{2+}]_{ex}$, which increased with exocytosis of Ca^{2+}-rich granules (Figure 7d).[41]

The characteristics of a variety of prevailing optical-based Ca^{2+} indicators and CSM techniques are summarized in **Table 2**. In brief, CSMs are capable of probing $[Ca^{2+}]$ in a range of nM to mM.[106] Their sensing principle avoids the issues of photobleaching and diffusion that affect fluorescence-based indicators. CSMs thus permit a stable, long-term tracking of $[Ca^{2+}]_{ex}$. In view of the large tip size and possible mechanical damage to cells, the CSM-based sensing

technique is preferable for measurements in the interstitial space.[107] The measurements mainly relate to the vicinity of the tip, so they do tend to be spatially limited.

Table 2. Summary of conventional Ca^{2+} sensors for islet studies

	Synthetic indicators	GECIs		CSMs
		Recombinant Aeq	Fluorescent proteins	
$[Ca^{2+}]$ sensing (μM)	0.04 – 1 [43, 83a, 108]	50 – 500 or 0.1 – 70 [49]		500 – 1500 [41]
K_d (μM)	0.06 – 0.39 [86, 109]	0.2 – 50 [109]	1.7 – 1000 [24a, 110]	10^{-4} – 10^{2} [111]
Signal strengths	●●●●●	●	●●●	●●●●
Advantages	- high signal-noise ratio - good localization - instantaneous response	- free from excitation light - precise localization - low photobleaching	- precise localization - low photobleaching - highly selective	- stable signal reading - good selectivity
Limitations	- photobleaching - prone to aggregate - non-specific binding	-non-ratiometric - very poor signal	- pH-sensitive - relatively weak signal	- low spatial resolution - concern of mechanical damages by oversize tip - slow response to Ca^{2+}

4. The state-of-the-art sensors for $[Ca^{2+}]_{ex}$

The potential for $[Ca^{2+}]_{ex}$ to coordinate intercellular signalling has given rise to the demand for sensors for *in situ* real-time tracking of $[Ca^{2+}]_{ex}$. An ideal sensor for this purpose should: (i) accurately quantify $[Ca^{2+}]_{ex}$ in the order of mM i.e., with a high-value K_d (or low affinity to Ca^{2+}); (ii) faithfully discern small fluctuations of $[Ca^{2+}]_{ex}$ from the high basal level, e.g., up to hundreds of μM changes over around 1.2 mM extracellular Ca^{2+}; (iii) selectively and instantaneously respond to Ca^{2+}; and (iv) track $[Ca^{2+}]_{ex}$ over a protracted period. In addition, the increasing demands for multiplexed sensing require high compatibility of indicators for both $[Ca^{2+}]_{ex}$ and other related bioactive molecules. In this section, we review the sensors that meet these criteria despite their applications may not be prevailing in islet study.

4.1 Chemically synthesized low-affinity Ca^{2+} indicators

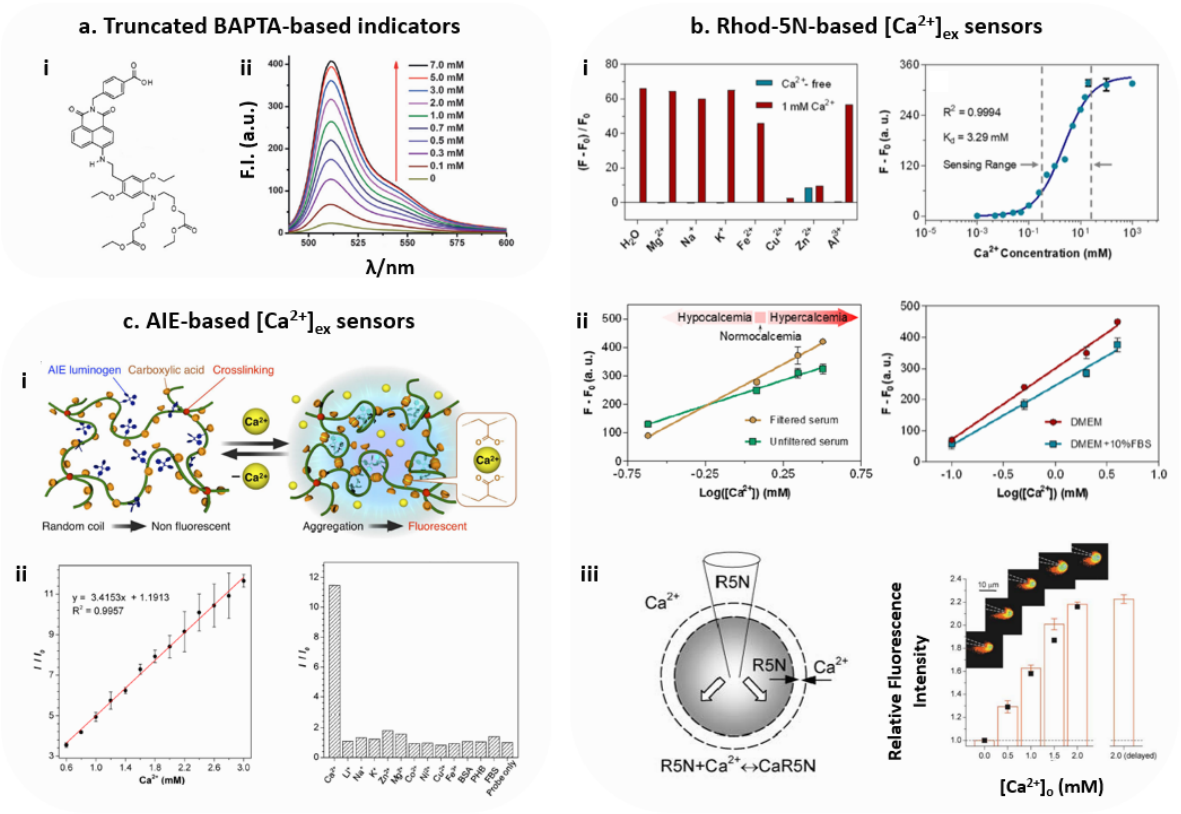

Figure 8 | Emerging low-affinity Ca^{2+} indicators for measuring high $[Ca^{2+}]$. a | i | A truncated BAPTA-based low-affinity Ca^{2+} indicator. As illustrated, the molecular structure (left) consists of Ca^{2+} recognition units and a fluorophore (4-amino-1,8-naphthalimide). Reproduced with permission.[112] Copyright 2008, Elsevier; The optical responses (λ_{ex}=477 nm) of truncated BAPTA in HEPES buffer (pH 7.4) upon addition of a series of Ca^{2+} stimuli. Reproduced with permission.[113] Copyright 2016, Wiley; **b | i |** Ion-selectivity investigation of Rhod-5N to Ca^{2+} in the presence of common extracellular cations, the concentrations of which were set to mimic the extracellular environment, including Mg^{2+} (1 mM), Na^{+} (150 mM), K^{+} (5 mM), Fe^{2+} (50 μM), Cu^{2+} (50 μM), Zn^{2+} (50 μM), and Al^{3+} (50 μM). The data represent relative fluorescence changes $(F - F_0)/F_0$ of 50 μM Rhod-5N with (red bars) and without (blue bars) addition of Ca^{2+} ($\lambda_{ex}/\lambda_{em}$ = 530/580 nm), where F and F_0 are the fluorescence of Rhod-5N in the presence and absence of the respective metal ions (left). The titration curve of 50 μM Rhod-5N, obtained by fitting its fluorescence at 580 nm (with Ca^{2+} from 1 μM to 1 M in the cell culture medium at 37 ℃) via Hill's equation, where Hill's coefficient (n_h) was determined as 0.94 ± 0.06, and K_d as 3.29 ± 0.41 mM, with an R^2 of 0.9994 (right). **ii |** Sensing $[Ca^{2+}]_{ex}$ in biomedical scenarios: Fluorescence of Rhod-5N increases linearly in response to a wide range of $[Ca^{2+}]$ in unfiltered and filtered human serum samples (left). $[Ca^{2+}]$-dependent fluorescence enhancement of Rhod-5N in Dulbecco's Modified Eagle Medium (DMEM) with and without fetal bovine serum (FBS, 10%) (right). Reproduced with permission.[15] Copyright 2020, American Chemical Society. **iii |** A micro-pipette probe filled with 3 mM Rhod-5N for sensing extracellular Ca^{2+} (left). The probe displays a linear fluorescence signal change in response to $[Ca^{2+}]$ from 0 to 2 mM (right). Reproduced with permission.[114] Copyright 2008, Elsevier. **c | i |** Schematic illustration of one aggregation-induced emission (AIE)-based fluorescent indicator (g-PAA-TPE) for Ca^{2+} sensing. Reproduced with permission.[115] Copyright 2016, Springer

Nature. **ii** | Relative fluorescence intensity changes of SA-4CO_2Na at 560 nm as a function of different [Ca^{2+}] (left); Relative fluorescence of SA-4CO_2Na in response to various metal ions and biological molecules in phosphate-buffered saline (PBS) (right): Ca^{2+} (3.0 mM), Li^{+} (1.0 mM), Na^{+} (150 mM), K^{+} (150 mM), Zn^{2+} (50 μM), Mg^{2+} (2.0 mM), Co^{2+} (50 μM), Cu^{2+} (50 μM), Fe^{3+} (50 μM), [Bovine serum albumin, BSA] = [Porcine haemoglobin, PHB] = [FBS] = 0.05 mg/mL, [SA-4CO2Na] = 1.0 mM; $\lambda_{ex}/\lambda_{em}$ = 351/560 nm. Reproduced with permission.[116] Copyright 2018, American Chemical Society.

A simple way to develop low-affinity indicators is to engineer conventional chemically synthesized indicators by reducing the ratio of Ca^{2+} binding sites (e.g., the carboxylic group) to its fluorophore molecules. A typical example is to truncate the carboxylic groups of the BAPTA-based indicators, which usually comprise four carboxylic groups for binding Ca^{2+}.[86, 117] The truncated indicator developed by He *et al*. exhibits increased fluorescence intensity by ~34% per 1 mM Ca^{2+} in the range of 0.3-2.2 mM (**Figure 8a, i left**), and also maintains the high selectivity for Ca^{2+} over Mg^{2+}.[112] An alternative method is to increase the ratio of fluorophores to the binding sites. For example, conjugation of an increased amount of fluorophore, BODIPY (4,4-difluoro-4-bora-3a,4a-diaza-s-indacene) with the truncated BAPTA resulted in an indicator with K_d up to ~0.92 mM and high selectivity for Ca^{2+} (about 9 times over other metal ions under physiological conditions) (Figure 8a, ii right).[113]

Other than modifying the BAPTA-based Ca^{2+} indicators, the renaissance of chemically synthesized indicators for extracellular Ca^{2+} also deserves attention. Of a list of commercial Ca^{2+} indicators, Rhod-5N emerges as a promising low-affinity Ca^{2+} indicator (K_d~0.32 mM, as specified by the manufacturer) for sensing $[Ca^{2+}]_{ex}$. The apparent K_d of Rhod-5N was increased to 3.29 mM in the cell culture medium (Dulbecco's Modified Eagle Medium, DMEM) where the high selectivity to Ca^{2+} was not compromised $^{+}$ (Figure 8b, i). This suggests that Rhod-5N is suitable for measuring Ca^{2+} between 0.33-33 mM, a range covering both physiological and pathophysiological variations in $[Ca^{2+}]_{ex}$. Moreover, the sensing profile of Rhod-5N for Ca^{2+} was retained in both raw and filtered human serum samples (Figure 8b, ii left). In DMEM or DMEM+10%FBS mixture (Figure 8b, ii right), the fluorescence enhancement of Rhod-5N exhibited a linear dependence on logarithmic [Ca^{2+}].[15] The work by Rusakov and Fine demonstrated that the fluorescence of Rhod-5N responded to 0-2 mM [Ca^{2+}] in an almost linear pattern, with ~ 2% increase per 100 μM.[114] This was realized by encapsulating Rhod-5N (dispersed in a Ca^{2+}-free buffer) into a concentric shell attached to a micropipette with tip size 2-3 μm (Figure 8b, iii left). A constant pressure was applied to the pipette to hold the Rhod-5N

buffer at the tip. Upon contact with Ca^{2+}-containing aqueous solvent, fluorescence at the tip area increased in response to the diffusion of Ca^{2+} into the shell (Figure 8b, iii right).

Aggregation-induced emission (AIE) fluorogens-based Ca^{2+} indicators are another emerging sensor for measuring [Ca^{2+}]. When embedded into Ca^{2+}-chelating ligands, AIE fluorogens emits fluorescence upon aggregation of fluorogens induced by Ca^{2+}. As illustrated in Figure 8c, i, one such sensor can be synthesized from chelator-conjugated polyacrylic acid (PAA) and AIE fluorogen tetraphenylethene (TPE) into a polymer gel form. In the presence of Ca^{2+}, the conformational changes of PAA pull the TPE appendants closer to trigger fluorescence.[118] Subject to the relative amount of TPE content (x), K_d of PAA-TPE_x varies from 0.43 to 2.8 mM. For example, g-PAA-$TPE_{0.02}$ exhibits 10% and 3% changes in fluorescence intensity when [Ca^{2+}] oscillates between 0.1-1.1 mM or 1.1-1.3 mM, respectively. Of note, the optical signal strength drops by ~ 20% after 5 cycles (about 25 minutes).[115] SA-4CO_2Na represents another AIE-based Ca^{2+} indicator, which is similarly generated by incorporating the AIE fluorogen salicyladazine (SA) into the negatively charged iminodiacetate groups (Ca^{2+} chelator). Upon exposure to Ca^{2+}, SA-4CO_2Na forms highly emissive fibrillary aggregates, leading to a linear increase in fluorescence over 11 fold in response to increasing [Ca^{2+}] from 0.6 to 3 mM (Figure 8c, ii left). SA-4CO_2Na also shows a high selectivity to Ca^{2+} over other metal ions and biomolecules (Figure 8c, ii right). Furthermore, SA-4CO_2Na remains viable for sensing Ca^{2+} in solid analytes, including psammomatous meningioma slice, microcracks on bovine bone surface and micro-defects on a hydroxyapatite-based scaffold.[116]

The sensors that have been developed to probe serum/blood Ca^{2+} represent a less explored group for tracing $[Ca^{2+}]_{ex}$. Moirangthem *et al* showed that a cholesteric liquid crystalline (CLC) polymer film could sense [Ca^{2+}] in the range of 0.1-10 mM. The polymer film utilized benzoic acids as metal-binding sites, and the emission of the film exhibited a blue shift in response to Ca^{2+} as the wavelength changed from green to blue ($\Delta\lambda$=70 nm). The Ca^{2+}-induced wavelength corresponded to distinct color changes, making the application of this film suited for rapid detection of blood Ca^{2+}, e.g., diagnosis of hypocalcemia or hypercalcemia.[119] Ding *et al*

utilized 3-aminopropyltriethoxysilane-coupled carboxylic acid (APS-CCA) to sense Ca^{2+} in the blood, and observed that the fluorescence of APS-CCA increased over 2 fold in response to 2 mM Ca^{2+}. The fluorescence response to other metal ions was negligible even at a supraphysiological level (2 mM). Incorporation of APS-CCA with a hydrophobic substrate-based microarray results in a high-throughput fluorimetric microarray, which facilitates high-throughput screening of blood Ca^{2+} (0.01-2 mM, over 20 blood samples in one measurement), with a sensitivity of 0.005 mM.[120]

4.2 Nano-structured sensors for $[Ca^{2+}]_{ex}$

Nano-structured Ca^{2+} sensors are an array of hybrid materials that can convert the change of $[Ca^{2+}]$ into discernible optical, electrical or magnetic signals. The signal type and detection range of these sensors depend on the modality of the nanomaterials and the binding affinity of the chelators. There is a growing list of nano-structured sensors that meet the requirement for measuring $[Ca^{2+}]_{ex}$.[121] In this sub-section, we focus on the nano-structured Ca^{2+} sensors of low binding affinity.

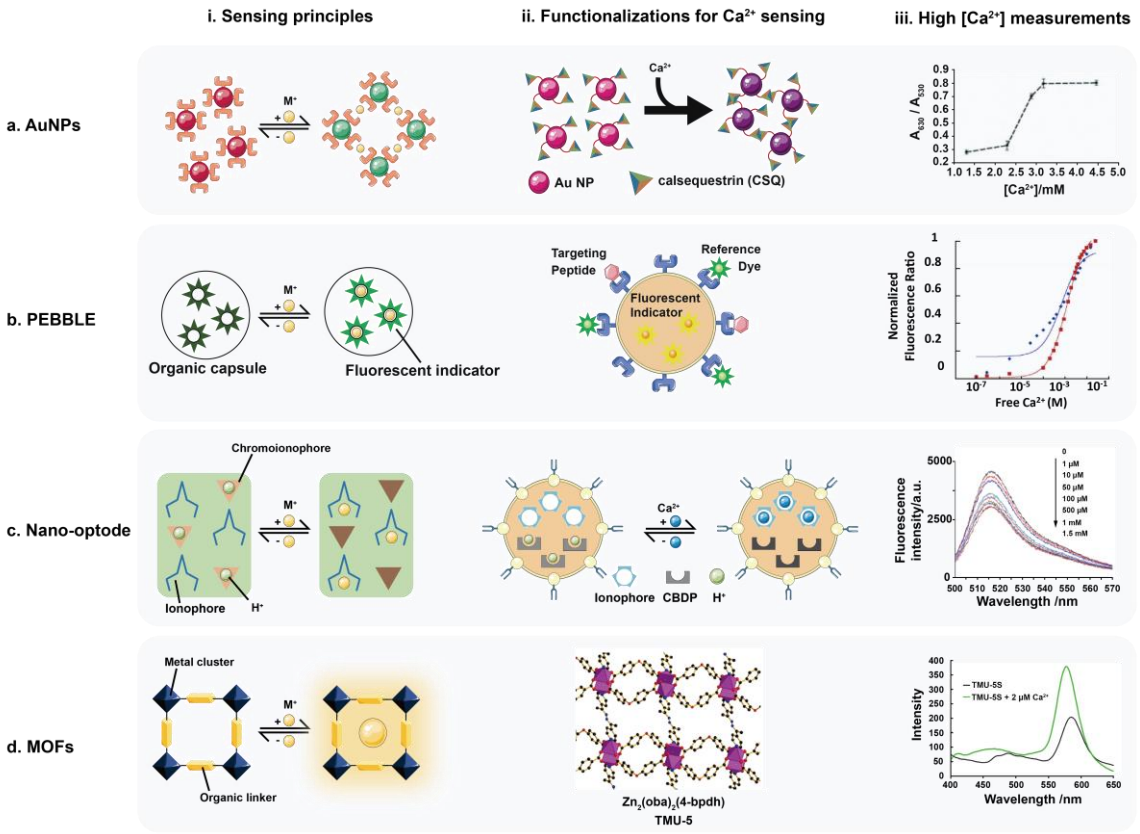

Figure 9 | Nano-structured Ca^{2+} biosensors. a | i | Sensing mechanism of Ca^{2+} chelator-functionalized gold nanoparticles (AuNPs). The presence of Ca^{2+} induces aggregation of NPs, leading to the SPR peak shift and color change. **ii |** Illustration of the process that calsequestrin (CSQ)-functionalized AuNPs undergo aggregation and exhibit colorimetric responses in the presence of Ca^{2+}. **iii |** Correlation of the ratio change of absorbance at 630 and 530 nm (A_{630}/A_{530}) as a function of [Ca^{2+}]. Reproduced with permission.[122] Copyright 2009, Wiley. **b | i |** Sensing mechanism of Ca^{2+} probes encapsulated by biologically localized embedding (PEBBLE), in which the fluorescence of the indicator increases upon binding to Ca^{2+}. **ii |** A representative PEBBLE sensor constructed by anchoring a reference dye, such as Hilyte, onto the surface of the polymer matrix, for ratiometric sensing capacity for Ca^{2+}. **iii |** Fluorescent responses of Rhod-dextran/Hilyte (blue) and Rhod-5N/Hilyte (red) PEBBLEs as a function of [Ca^{2+}]. Reproduced with permission.[123] Copyright 2012, American Chemical Society. **c | i |** Sensing mechanism of a nano-optode constructed by Ca^{2+}-selective ionophore and pH-sensitive chromoionophore. **ii |** Ion-exchange process in a polymeric lipophilic nanospheres embedded with Ca^{2+}-selective ionophore (ETH 129) and chromoionophores (calix[4]arene-functionalized bodipy, CBDP). The ionophore selectively transports Ca^{2+} into the nanosphere in exchange with H^+, leading to a change in the fluorescence of CBDP. **iii |** The emission spectra of CBDP-encapsulated nanospheres as a function of [Ca^{2+}] from 1μM to 1.5 mM in PBS solution, pH 7.4 ($\lambda_{ex}/\lambda_{em}$=480/516 nm). Reproduced with permission.[124] Copyright 2016, American Chemical Society. **d | i |** Sensing mechanism of metal-organic frameworks (MOFs). The optical property of MOFs is susceptible to the conformational changes induced by the guest metal ions. **ii** | Structure of $Zn_2(oba)_2(4\text{-bdph})$ TMU-5, a Ca^{2+}-responsive MOFs: 6-coordinated $Zn_2(-COO)_4(-PY)2$ paddlewheel secondary building units are linked via oba and 4-bpdh

ligands resulting in three-dimensional azine-functionalized interconnected pores; **iii |** Emission spectra of TMU-5S dispersed in distilled water with and without 2×10^{-6} M Ca^{2+} (λ_{ex}=355 nm). Reproduced with permission.[125] Copyright 2020, American Chemical Society.

For gold nanoparticles (AuNPs), the specific electromagnetic fields (e.g., incident light) acting on the particles can drive resonant oscillations of electrons of the conductor at the NP interface, namely surface plasmon resonance (SPR) characteristic, which has been utilized for sensing provided that there are analyte-induced changes at the NP-environment boundary (e.g., variations in the size and shape of AuNPs and absorption of molecules onto the surface).[126] In general, SPR wavelength shift reflects such variations. As exemplified in **Figure 9a, i**, Russell *et al*. functionalized AuNPs with carbohydrate moieties (lactose), and showed that the degree of AuNP clustering and associated colorimetric changes were dependent on [Ca^{2+}] in the range of 0.8-2.2 mM (overlapping part of physiological $[Ca^{2+}]_{ex}$) and 10-35 mM. The authors suggested that the sensing range is closely related to the length of the linker that bridges AuNPs and the chelator, such as ethylene glycol.[127] As shown in Figure 9a, ii and iii, calsequestrin (CSQ)-AuNPs aggregate in the presence of Ca^{2+} (but not other metal ions) and undergo a linear colorimetric shift when serum Ca^{2+} changes from 2.4 to 3.5 mM.[122]

Another development of nano-structured Ca^{2+} sensors is largely driven by their capacity for assembling or encapsulating fluorescent Ca^{2+} indicators into a nanoscale matrix.[128] Its salient feature includes protection of the indicators from unwanted interferences of the surroundings and acting as new carriers for delivery.[129] Compared to native indicators, the nanoscale capsule may mitigate the photobleaching issue (e.g., negligible impairment over a 40-minute exposure to UV light) and reduce the leaking rate (<3% leakage over 24 hours).[130] One construction is to encapsulate the probes with biologically localized embedding (PEBBLE) (Figure 9b, i), where polyacrylamide or poly-(decylmelacrylate) works as the matrix to accommodate different Ca^{2+} indicators, such as Rhod-2,[123] Calcium Green[131] or Fluo-4.[132] PEBBLE nanosensors with dimensions of 20 to 600 nm, have been generated for detection of various bioactive molecules, including cellular Ca^{2+} (Figure 9b, ii). As shown in Figure 9b, iii, a PEBBLE nanosensor incorporating Rhod-5N exhibits a K_d of ~1.25±0.006 mM, which is suitable for measuring high [Ca^{2+}].[123] Such nano-structured Ca^{2+} sensors are also generated by utilizing silica NPs as the host matrix. Conjugation of dextran-encapsulated silica NPs with both the Fluo-4 and a reference dye can generate a ratiometric sensor that responds to Ca^{2+} up

to 50 μM.[133] Its sensing range can be enlarged by replacing Fluo-4 with a low-affinity Ca^{2+} indicator, e.g., Calcein.

More recently, nano-structured optical Ca^{2+} sensors have also emerged from ion-selective nano-optodes, which are composed of Ca^{2+}-responsive ionophores (that are often used in CSM), ion-exchanger and lipophilic-sensing components (chromoionophore), such as a pH indicator, in a polymeric lipophilic matrix.[134] As depicted in Figure 9c, i, the ionophores selectively transport Ca^{2+} into the optode, driven by the concentration gradient. Subsequently, H^+ is released to maintain the electroneutral state inside. As a consequence, the internal pH of the sensor changes, which further influences the optical properties of the embedded lipophilic-sensing components (e.g., chromoionophore). Figure 9c, ii illustrates a representative of Ca^{2+}-responsive nano-optode, which consists of Ca^{2+} ionophore II (ETH 129) and chromoionophore calix[4]arene-functionalized bodipy (CBDP). In response to [Ca^{2+}] from 1 μM to 1 mM, this sensor shows a gradual decrease in fluorescence intensity (Figure 9c, iii). Similar to PEBBLE sensors, the encapsulation of nano-optode in a polymer also prevents disturbance from the environment, which is advantageous for tracing [Ca^{2+}] over a prolonged period of time. The other nano-optode sensors, containing either CBDP or 9-(diethylamino)-5-[(2-octyldecyl)imino]benzo[a]phenoxazine (ETH 5350) as chromoionophore, exhibit stable fluorescence in the first 3 hours after being loaded into Hela cells (an immortal cell line derived from human cervical cancer), followed by around 40% decrease over 24 hours.[124] The sensing range of nano-optodes appears to depend on the binding affinity of the Ca^{2+}-selective ionophore. Therefore, the effective sensing range is flexible to be tuned for different sensing purposes, including measurement of $[Ca^{2+}]_{ex}$ by adopting low-affinity ionophores. In comparison to CSM, the response time of nano-optode is improved by orders of magnitude, as short as ~1 s to date, but this remains barely competitive with the temporal resolution of chemically synthesized or protein-based Ca^{2+} indicators. Such a temporal resolution may result in the distortion or dismissal when extracting transient Ca^{2+} signals.

An emerging high-performance sensor is based on metal-organic frameworks (MOFs), a type of crystalline solid constructed by connecting metal cations or groups of cations (nodes) via organic ligands (linkers that have multiple binding sites) to form single- or multi-dimensional extended coordination networks.[135] Of note, MOFs fluoresce upon excitation of either metal components or organic ligands. In addition, optical characteristics of MOFs are dependent on node-to-ligand or ligand-to-ligand interaction, or the interaction between MOFs and the surrounding environment.[136] With different pore sizes and combinations of metal ions and

ligands, it is feasible to customize MOFs to sense various molecules that are smaller than the pore of MOFs (Figure 9d, i).[137] For example, Ca^{2+}-responsive MOFs have been developed from a three-dimensional lanthanide anionic structure based on $\{K_5[Tb_5\text{-}(IDC)_4(ox)_4]\}_n \cdot n_3(20H_2O)_n$. K^+ in its one-dimensional channel can exchange with Ca^{2+} to induce a remarkable increase in fluorescence at ~480 and 550 nm. However, these MOFs also respond to other metal ions, such as Fe^{2+} and Cu^{2+}.[138] The poor selectivity towards Ca^{2+} thus restricts their biological application. Figure 9d, ii shows the spectra of a MOF-based ratiometric Ca^{2+} sensor, TMU-5S, $[Zn(C_{14}O_5H_8\,(C_{14}H_{14}N_4)_{0.5}] \cdot (C_3NOH_7)_{1.5}(RhB)_{0.002}$, which was synthesized by integrating rhodamine B with the MOF. Upon addition of 2 μM Ca^{2+} (in a cell-free experimental setup), the fluorescence of TMU-5S increased, in association with a blue shift (from 485 nm to 465 nm, and from 585 nm to 575 nm, respectively) (Figure 9d, iii). The results also showed that TMU-5S preferentially binds to Ca^{2+} over other metal cations at physiological concentrations, and exhibits a 5-second response (the time required to obtain the 90% real value) and 40-second recovery (the time for releasing up to 90% from a specific target).[125] The temporal responsiveness is sufficient for tracing slow Ca^{2+} changes, but may be too protracted for fast-tracking or instantaneous reading of $[Ca^{2+}]$ changes.

4.3 Microfluidics-based multiplexed sensing platforms

A microfluidic sensing platform typically comprises three core modules: perfusion controller(s), customized microfluidic chip and (multi-) analytical station(s).[139] The perfusion system customizes the perfusion rate, in the micro- or nano-liter range per minute, via peristaltic pumps (for long-term perfusion) or syringe pumps (for short-term perfusion). The second component, a microfluidic chip, is central in the system. It incorporates the mechanism to immobilize biological samples and provides samples with a biomimetic environment, while the channel structures in the microchip regulate the shear stress that the trapped tissues are exposed to, which impacts the viability of the tissues to be studied. Moreover, the microfluidic chip features the flexibility and compatibility required for simultaneous multiplexed tracing of bioactive molecules. Subject to the specific research question, analytical modules such as optical microscope and on-chip immunoassay based on antigen-antibody reactions can be incorporated, allowing for tracking small molecules (e.g., ions and ATP) or large biomolecules (e.g., peptide and protein).

For the first module, the selection of the perfusion controller is based on the perfusion requirements as mentioned in the preceding paragraph. The major variation between microfluidic chips lies in the design of the microchannels and trapping structures, which should ensure effective capturing and immobilization of the samples of interest, e.g., the primary pancreatic islets and islet spheroids.

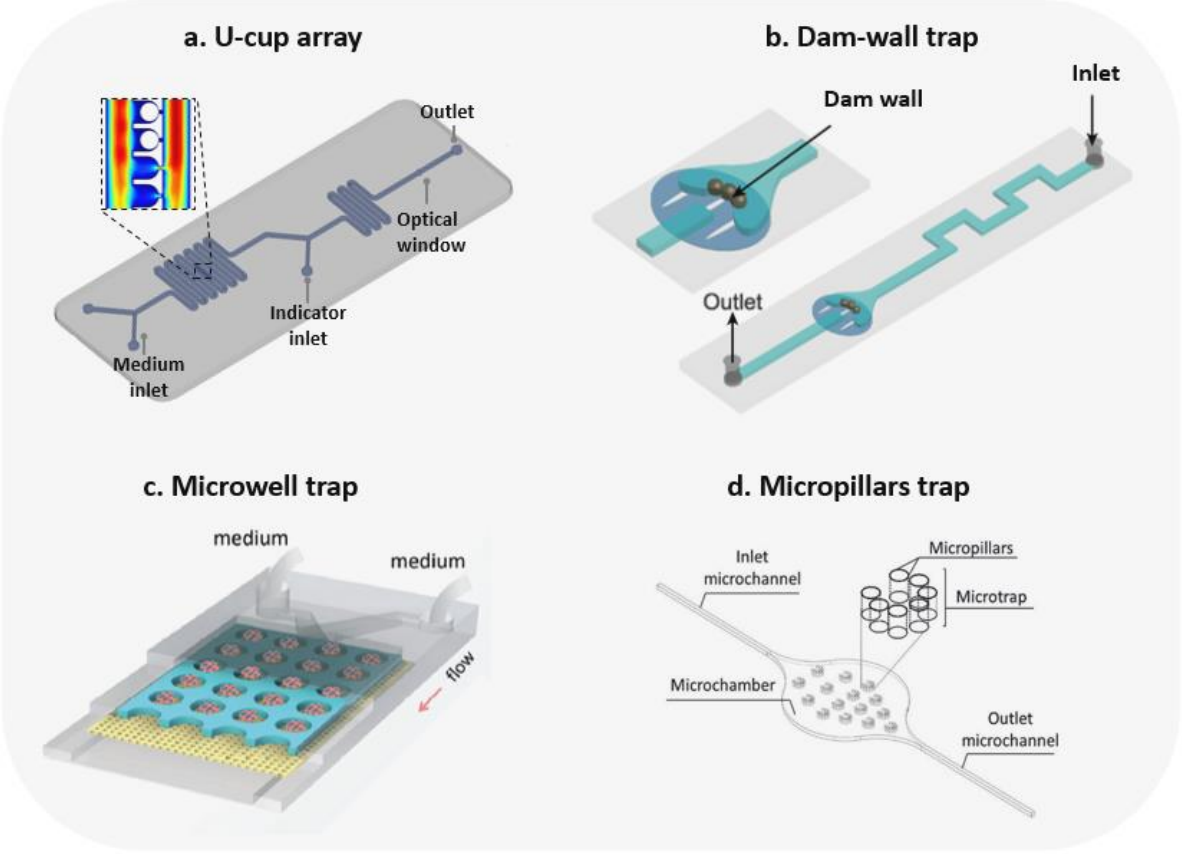

Figure 10 | Illustration of selected microfluidic chips. a | Layout of a U-cup based microfluidic chip, with two Y-shape inlets, two sections of serpentine channel, a column of U-cups, an optical window and an outlet. Reproduced with permission.[15] Copyright 2020, American Chemical Society. **b |** A schematic of a microfluidic device that utilizes a dam-wall design to capture pancreatic islets. Islets and media are delivered into the device by flow from the inlet to outlet ports with tubing. This two-layer device contains a 125 μm tall main channel and 25 μm tall dam wall. The schematic of the zoomed-in holding area shows that islets in this channel are prevented from moving down the channel by the drop in height. This design maintains the islets stationary with flow directed at the islets. Reproduced with permission.[140] Copyright 2013, Royal Society of Chemistry. **c |** Schematic diagram of organoids on the chip with well traps. The device consists of four parts: top and bottom PDMS layers separated by a through-hole PDMS membrane and a polycarbonate porous membrane. The microwell array of the upper layer allows the three-dimensional culture of islet organoids under dynamic medium perfusion. Polycarbonate porous membrane is applied to separate the media flow of the upper channel from the lower. Reproduced with permission.[141] Copyright 2019, Royal Society of Chemistry. **d |** Layout of a microfluidic system with microchamber for the collection and culture of multiple islet cells. The culture chamber consists of 15 round

microtraps (280 μm × 280 μm) and 7 micropillars each (145 μm × 145 μm × 200 μm), which support the construction of islet-like tissue (islet diameter ~185 μm). Reproduced with permission.[142] Copyright 2019, Elsevier.

Figure 10 illustrates four types of frequently adopted tissue trapping structures in microfluidic sensing platforms. Under hydrodynamic force, the U-cup tissue array is able to sequentially immobilize individual primary pancreatic islets in each cup while reducing the shear stress imposed on the trapped tissue via directing the branch of the perfusion flow into the cup (Figure 10a).[15, 143] The U-cups are selective for islets with a specific range of dimensions, as the smaller islets would either escape the capture of the cup via the neck or stack within the cup, while the larger ones drift downstream along the channel and are not directed into the cup. Regarding the other chambers, a dam-wall like tissue chamber is preferable to load tissue of different sizes, despite that the flow imposed on the trapped islets has been shown to dampen the glucose-stimulated Ca^{2+} response of the periphery of the islet where fluid shear stress is greatest (Figure 10b).[144]

In addition to acting as trapping sites for primary tissues, the chambers are adaptable to enable the on-chip formation of islet organoids/spheroids. As shown in Figure 10c, the microwell chambers have been used to host islet organoids that grow from stem cells captured from the perfused medium by gravity.[141] It has been suggested that the capturing function of wells is consistent when the flow rates are less than 2 μL/min, which however may be too slow to grow healthy organoids.[145] Though the fabrication of the microwell is relatively simple, the challenge lies in the uneven provision of nutrients in the well, because the fluid exchange at the bottom is much slower than on its surface.[146] To mitigate these issues, a microchamber with 15 microtraps based on 7 circularly patterned micropillars was developed, allowing for efficient exchange of interstitial fluid and capturing of the suspended cells in a perfused medium (e.g., 2×10^6 cells/mL) (Figure 10d). The fluidic dynamic simulation suggested there is a stable, uniform flow with negligible shear stress in these microtraps. This may account for well-differentiation and high survival rates of islet organoids in the micropillar trap – over 72-hour culturing, 85% of cells are viable in the micropillar trap in contrast to 45% in the microwell trap).[142]

As introduced in Section 2, insulin secretion is initiated by multi-step intracellular Ca^{2+} signalling and synchronized by intercellular communication. Multiplexed sensing is in great demand, to provide a comprehensive understanding of the steps involved, since it carries the

following advantages: (i) it provides biologically relevant perfusion and enables organ-crosstalk that mimics *in vivo* conditions; (ii) it is compatible with different sensing agents and modules, allowing for simultaneous monitoring of multiple bioactive molecules that are involved in insulin secretion; and (iii) it has the flexibility to include temporal and spatial sensing modalities that are needed for precise comprehension of a signalling network.

Provision of dynamic and bio-mimicking environments for the immobilized islets in a microfluidic chip is advantageous for maintaining the viability and bioactivity of islets in response to stimuli. In contrast to conventional culture in a petri dish, the application of a microfluidic setup was shown to preserve the GSIS from around 72 hours to over 240 hours.[147] However, the disruption of the capillary vascular system of isolated islets is unlikely to be compensated solely by providing a biomimetic perfusion environment.[148] As such, there is growing research into incubating islet-like tissues in the microfluidic chip, such as islet micro-tissues and islet spheroids (organoids) from dispersed primary islet cells and pluripotent stem cells, which retain the biological features of primary islets, including islet morphology, cellular composition and secretory profiles.[149] Consequently, the observation window for evaluation of islet function can be extended to 28 days for the islet micro-tissue[149] and 45 days for islet spheroids.[141] On the basis of a dam-wall islet trap, a microfluidic chip system has been developed to provide glucose at either a constant or pulsatile rate with varying amplitudes (0.5, 1, 1.5 on the basis of 11 mM mean glucose level) and periodicities (spanning from 20 to 2 minutes). Upon these varied waveforms, $[Ca^{2+}]_c$ resonates and reaches the apex of its oscillation only when glucose is perfused with a periodicity resembling *in vivo* glucose oscillation (around 5-10 minutes per cycle).[30c, 150] The improved responsiveness to glucose is further supported by the amplified insulin release at the second phase of GSIS under the same pattern of glucose stimulation.[68]

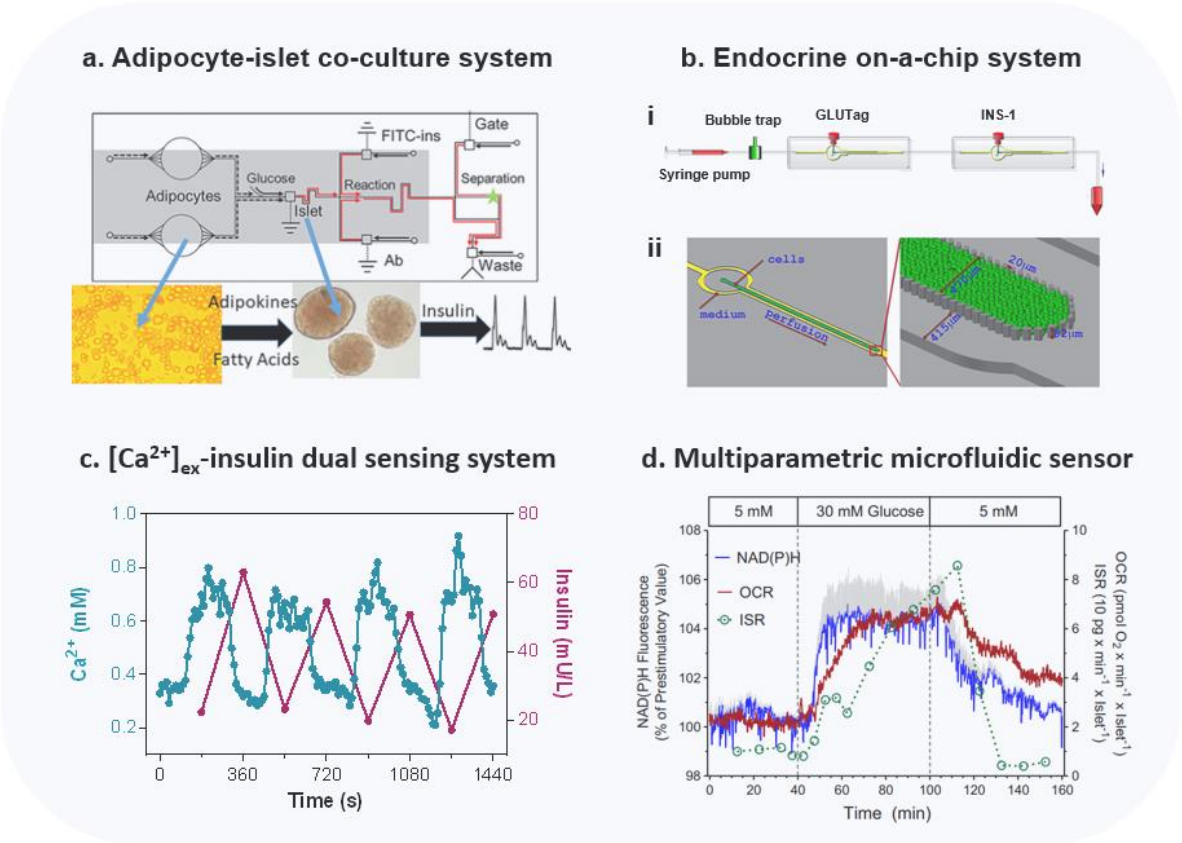

Figure 11 | Multiplexed microfluidic sensing systems. **a |** Top view of a microfluidic chip for investigation of the role of adipocytes in the control of islet function. Solid lines indicate the microfluidic channels. The large circles on the left represent the adipocyte chambers drilled through the glass (light image of adipocytes shown underneath). The shaded section of the chip indicates the parts that are heated during experiments. In this setup, the perfusate containing adipocyte-derived secretory products (dashed lines) is delivered into the islet chamber together with glucose from the side channel. Insulin secretion from the islets is monitored by electrophoretic competitive immunoassays, for which fluorescence labelled insulin (FITC-ins) and insulin antibody are infused into the channel guided by electro-osmotic flow (red arrow). The laser-induced fluorescence (LIF) detection point, sited 1 cm beyond the injection cross (indicated by the star), monitors the dynamic concentration of insulin secretion. Reproduced with permission.[151] Copyright 2018, American Chemical Society. **b |** Schematic of the endocrine system-on-chip. **i |** The cells are loaded into their respective chambers via a syringe pump. Culture medium is supplied via the inlet. The perfusate from the outlet is collected for further analysis. The two chambers are joined by a connection tube. **ii |** Dimensions of the three-dimensional microfluidic chip. Micropillars divide the microfluidic channel into a central cell culture compartment and two side channels for perfusion of the culture medium**.** Reproduced with permission.[152] Copyright 2017, IOP Publishing. **c |** Simultaneous monitoring of dynamic Ca^{2+} and insulin in a biologically relevant environment. Oscillatory patterns of both Ca^{2+} and insulin well align with the set frequency. The temporal delay between the two measurements reflects the time required for the perfusion flow to travel from the optical window (for measuring Ca^{2+}) to the channel outlet (for sample collection to measure insulin), which can be corrected based on the flow rate. Reproduced with permission.[15] Copyright 2020, American Chemical Society. **d |** Multiparametric microfluidic sensor for simultaneous

monitoring of various bioactive molecules during GSIS. The concentration of glucose is set to vary between 5 and 30 mM. Multiplexing is achieved by incorporation of respective indicators, i.e., NAD(P)H (blue trace) via autofluorescence, $\lambda_{ex}/\lambda_{em}$=366/450 nm, oxygen consumption rate (OCR) via implanted miniaturized oxygen probe, and insulin secretion rate (ISR) via enzyme-linked immunosorbent assay (ELISA). Reproduced with permission.[146] Copyright 2017, Springer Nature.

The microfluidic chip is also a unique sensing platform for the investigation of organ crosstalk that may participate in the regulation of insulin secretion. In the body, adipocytes secrete nonesterified fatty acids (NEFAs) that have been shown to exert a bimodal effect on insulin secretion, i.e., short-term exposure (less than several hours) to NEFAs enhances insulin secretion[153] while chronic exposure (over 1-2 days) suppresses it.[154] It is difficult to gain in-depth knowledge on the dynamic interaction between adipocytes and pancreatic islets based on the conventional static incubation method. As shown in **Figure 11a**, adipocytes (3T3-L1, a mouse adipose cell line) and primary mouse islets can be co-cultured in a microfluidic sensing platform. In this setup, Lu *et al* demonstrated that signals derived from adipocytes in the upper stream of the perfusion augmented glucose-induced (11 mM) insulin secretion from the downstream islets substantially.[151] Likewise, the gut-derived incretin hormone, glucagon-like peptide 1 (GLP-1), stimulate insulin secretion in a glucose-dependent manner. GLP-1 mimetics are now a mainstay in the management of T2DM.[155] Screening for effective stimuli for GLP-1 secretion represents an approach to identifying new therapies for T2DM.[156] To this end, a microfluidic chip system was developed to co-culture GLUTag cells (GLP-1 secreting cells) and INS-1 cells (β cell line) (Figure 11b). The functionality of the cultured cells in the two chambers was evaluated independently by measuring insulin and GLP-1 secretion when the glucose concentration was increased from 3 to 20 mM. The results showed that insulin secretion was increased by around 5 ng/10^6 cells on the INS-1 chamber and GLP-1 secretion by 0.6 ng/10^6 from the GLUTag chamber. In addition to glucose concentration, the flow rate also influenced the secretion of both hormones, as insulin and GLP-1 increased from 21 to 32 ng/10^6 cells and from 0.6 to 4.8 ng/10^6 cells, respectively, when the perfusion rate was increased from 2 µL/min to 10 µL/min. This study further demonstrated that the co-culture with GLUTag cells improved the insulin output by around 1 ng/10^6 cells/minute compared with the culture of the INS-1 cells alone.[152] It should be noted that both of the cells used in the experiment were cancer cell lines, and the implications of these observations remain to be validated in primary tissues or animal models.

The microfluidic sensing system is characterized by high spatial and temporal resolutions for tracing multiple physiological factors through the integration of different analytical modalities. For example, our recent work (a pseudo-islet study) has shown concurrent measurements of $[Ca^{2+}]_{ex}$ and insulin concentration via integrating optical modalities for on-chip monitoring of Ca^{2+}-induced fluorescence of Rhod-5N and off-chip insulin quantification via enzyme-linked immunosorbent assay (ELISA). The temporal resolutions for measuring $[Ca^{2+}]_{ex}$ and insulin are 10s and 1 minute, respectively (Figure 11c).[15] In other work, a microfluidic chip was integrated with a fluorescence microscope for multiplexed imaging of Ca^{2+} (by Fura-2) and mitochondrial membrane potential (by Rh123) within the trapped islets. The concurrent monitoring of the excitation ratio of Fura-2 at 340/380 nm and the fluorescence of Rh123 at 535 nm revealed the dynamic changes of $[Ca^{2+}]_c$ and mitochondrial activity at the same time. These observations validated the feasibility of multi-parametric monitoring of signalling kinetics via an integrated system.[157]

Schulze *et al* developed a multiparametric microfluidic sensor for simultaneous monitoring of oxygen consumption, $[Ca^{2+}]_c$, insulin secretion and intracellular NAD(P)H, where insulin was measured off-chip by ELISA, and $[Ca^{2+}]_c$ and NAD(P)H were indicated by reading on-chip optical signals of Fura-2 and NAD(P)H (autofluorescence), respectively. The dynamic oxygen consumption was recorded by oxygen sensors (Pst3 sensor and Fibox4 meter) mounted on the inlet and outlet of the microfluidic chip. The pre-determined flow rate and perfusion distance would allow for temporal corrections for correlating the kinetics of molecules measured at different locations (Figure 11d).[146] When necessary, other analytical techniques, such as patch-clamp,[158] amperometry[159] and capillary electrophoresis immunoassay (CEI),[160] can be incorporated into the microfluidic system.[161]

5. Conclusions and Outlook

There is a wide recognition that Ca^{2+} acts as an indispensable messenger within and outside cells to signal cellular functions in a range of physiological and pathological processes,[162] including but not limited to immune responses,[163] brain function,[164] cancer,[165] cell death[166] and insulin secretion from pancreatic β cells.[167] In general, Ca^{2+} oscillates in different cellular domains as a result of dynamic Ca^{2+} exchange between intra- and extracellular compartments.

The increases in $[Ca^{2+}]_{mito}$ and $[Ca^{2+}]_{ER}$ are usually related to the uptake of cytoplasmic Ca^{2+} into mitochondria and ER. Oscillations of Ca^{2+} within each of these cellular compartments are intertwined with critical steps of, for example, pulsatile insulin secretion in response to glucose stimulation. Specifically, $[Ca^{2+}]_c$ participates in the firing of action potentials to trigger exocytosis of insulin granules. $[Ca^{2+}]_{mito}$ oscillation induces oscillatory production of ATP, while $[Ca^{2+}]_{ER}$ buffers the sharp change in $[Ca^{2+}]_c$ to maintain cell vitality. Within the pancreatic β cells, disruption of Ca^{2+} oscillations in the cytoplasm and mitochondria markedly attenuates pulsatile insulin secretion. Inhibition of Ca^{2+} transportation in ER, at least acutely in the first phase, augments $[Ca^{2+}]_c$ and insulin secretion. $[Ca^{2+}]_{ex}$ has also been found to be oscillatory in the vicinity of β cells under glucose stimulation, due probably to Ca^{2+} influx via VGCC (that decreases $[Ca^{2+}]_{ex}$) and Ca^{2+} extrusion pathways including exocytosis with insulin and export of cytoplasmic Ca^{2+} (that decrease $[Ca^{2+}]_{ex}$). There is increasing evidence suggesting that extracellular Ca^{2+} may signal intercellular communication via CaSR, a unique pathway that may be responsible for synchronization of insulin secretion between β cells. Hitherto, it remains to be elucidated as to what are the intrinsic pacemakers that dictate the frequency and amplitudes of Ca^{2+} oscillations, and the extent to which cytoplasmic Ca^{2+} shapes the pulsatility of insulin secretion.

Understanding of Ca^{2+} signalling has been paired with the advent and advancement of contemporary Ca^{2+} sensors and sensing methodologies. Since the first observation of dynamic changes in intracellular Ca^{2+} by a bioluminescent protein (i.e. Aeq), three major types of Ca^{2+} sensors have been established and widely used, including chemically synthesized fluorescent Ca^{2+} indicators, GECIs and CSMs. Abundant synthetic fluorescent Ca^{2+} indicators have provided options for the spectral property and binding affinity, which are particularly suitable for sensing cytoplasmic Ca^{2+}, albeit with limitations of poor localization and the issue of leaching within cellular domains. GECIs can be precisely expressed in a specific subcellular

compartment, but their organelle-targeting efficiency is often hampered by the expression level and maturation speed of the protein indicators.[100] Another aspect that may be overlooked is that fusion of GECIs with a tag sequence is likely to change their binding affinity (or K_d) towards Ca^{2+}. In situ fluorescence titration is thus recommended to re-determine the modified binding kinetics after the indicators are expressed in the cells. Such post-characterization is necessary to validate their ability to sense Ca^{2+} in the specific target domain. CSMs are of limited use for measuring intracellular [Ca^{2+}] due to their inevitable mechanical damage to the cell and are, therefore, mainly employed for monitoring $[Ca^{2+}]_{ex}$. However, CSMs are suitable for a point-of-care measurement, though not for mapping the kinetics or tracing the change of $[Ca^{2+}]_{ex}$ in multi-cellular or tissue level.

The demand for sensors competent for measurement of $[Ca^{2+}]_{ex}$ has stimulated the search for new-generation Ca^{2+} sensors or sensing methodologies. One straightforward strategy is to tune down the binding affinity of an indicator (e.g., BAPTA-based) to Ca^{2+}. This can be achieved by increasing the relative ratio of fluorophore to the Ca^{2+} binding sites, either by conjugating more fluorophore or truncating carboxyl groups (the binding sites) of the Ca^{2+} chelator, or both. In addition, Ca^{2+} chelator-conjugated AIE-based indicators have been synthesized with low binding affinity to Ca^{2+}. Both modified BAPTA-based and AIE-based Ca^{2+} indicators have a sensing range between 0.5 and 3 mM, which is suitable for measurement of $[Ca^{2+}]_{ex}$, while maintaining excellent Ca^{2+} selectivity over other physiological metal ions. Other than CSMs which measures electric potentials, optical indicators commonly face the issue of photobleaching, regardless of their applications for intra- or extracellular Ca^{2+}.

Recently, nano-structured Ca^{2+} sensors have been explored for sensing $[Ca^{2+}]_{ex}$. These sensors are typically based on the encapsulation/conjugation of Ca^{2+}-responsive materials into/onto materials at the nanoscale. The incorporation of diverse Ca^{2+} chelators and fluorophores into nano-materials has led to a series of Ca^{2+} sensors with varying K_d. Protected by biocompatible

and viable matrix materials, nano-structured Ca^{2+} sensors exhibit minimal cytotoxicity and high photobleaching resistance. However, their applications in the long-term tracing of cellular Ca^{2+} is still restricted due to the aggregation of nanomaterials that is difficult to avoid.

Given the intimate involvement of Ca^{2+} in the complex signalling network, the development of multiplexed platforms capable of sensing Ca^{2+} and other biological targets is of major interest. At a single cell level, multiplexed sensing has been achieved by simultaneously utilizing multiple indicators for different bioactive molecules including Ca^{2+}, ATP, pH and O_2, in combination with the autofluorescence of small molecules (e.g., NAD(P)H) and electrophysiological sensors (e.g., patch clamp). In the context of a group of cells or a tissue, microfluidic chips appear to be an advantageous sensing platform for at least three reasons. First, microfluidic chips, as opposed to the conventional sensing experiment in a static setup, e.g., a petri dish, generate a dynamic culture environment, including continuous provision of refreshed culture media and chemical/physical stimulation for the biological subject of interest, which better mimics the physiological environment.[156] As such, cultured cells or tissues experience improved viability and sustained functionality, and cellular responses obtained in such a biomimetic system are more likely to reflect actual reactions that would occur *in vivo*.[151, 152] Second, microfluidic chips have high combability with a variety of sensing modules, the integration of which have uncovered the links of dynamic intra- and inter-cellular Ca^{2+} signalling and metabolic activity (e.g., glycolysis and ATP production) with insulin secretion. However, photocytotoxicity could be a concern for multiplexed sensing studies in the case that the optical module is incorporated (where external light excitation is applied). Third, the microfluidic platform permits the reconstruction of cell-cell or even organ-organ crosstalk, allowing delineation of complex intercellular or inter-organ communication.

Despite not the focus of this review, the advanced optical microscopy techniques have also made a great contribution to the understanding of intracellular activities. For example, the

integration of laser-scanning microscopy and intravital microscopy with Ca^{2+} sensors (e.g., GECIs) has allowed for intracellular Ca^{2+} imaging in both transplanted islets[168] and endogenous islets[169] *in vivo*. Similarly, monitoring of Zn^{2+} release from beta cells by intravital microscopy has been shown to be useful to trace insulin secretion.[170]

Ca^{2+} signalling continues to be a major target of interest in various fields of biomedical research. In the study of islets, decoding Ca^{2+} oscillations is expected to reveal how the pulsatile insulin secretion is coordinated and what factors modify the secretory response. To date, understanding of Ca^{2+} signalling in live cells/organisms has mainly relied on the improvement of Ca^{2+} sensors. Emerging innovative Ca^{2+} sensing materials and platforms, represented by the low-affinity Ca^{2+} indicator, nano-structured Ca^{2+} and microfluidic sensing platforms, are able to unveil new roles of $[Ca^{2+}]_{ex}$, particularly in intercellular communication and synchronized cellular behaviors. The convergence of intra- and intercellular Ca^{2+} signalling may shed light on fundamental mechanisms relating to insulin pulsatility, which can potentially unlock useful therapeutic targets for T2DM.

Author Contribution

J. (T.) Z. and T. W. conceived and led the project. W. H., T. W. and J. (T.) Z. wrote and revised the manuscript. W. H. and C. X. prepared the tables and figures. C. X., C. K. R., C. P. and H. Ebendorff-Heidepriem revised the manuscript.

Acknowledgement

W. H. acknowledges the Adelaide Graduate Research Scholarship from the University of Adelaide, Australia. T. W. acknowledges a Mid-Career Fellowship from The Hospital Research Foundation and an Emerging Leaders Development Award from the University of Adelaide. This work is initiated and supported by Interdisciplinary Project Grant to J. (T.) Z., T. W., C. R. and H. E. from the University of Adelaide. This work was performed in part at the South Australia and Optofab nodes of the Australian National Fabrication Facility (ANFF) under the National Collaborative Research Infrastructure Strategy to provide nano- and microfabrication facilities for Australia's researchers.

Conflict of Interest

The authors declare no conflict of interest.

Reference

[1] a) M. J. Berridge, M. D. Bootman, H. L. Roderick, *Nature reviews Molecular cell biology* **2003**, 4, 517; b) O. H. Petersen, M. Michalak, A. Verkhratsky, *Cell calcium* **2005**, 38, 161; c) A. Semyanov, C. Henneberger, A. Agarwal, *Nature Reviews Neuroscience* **2020**, 21, 551.

[2] A. J. Kreutzberger, V. Kiessling, B. Liang, P. Seelheim, S. Jakhanwal, R. Jahn, J. D. Castle, L. K. Tamm, *Science advances* **2017**, 3, e1603208.

[3] B. K. Puri, *Calcium Signaling* **2020**, 537.

[4] Y. Yamada, K. Namba, T. Fujii, *Nature communications* **2020**, 11, 1.

[5] N. Mannowetz, M. R. Miller, P. V. Lishko, *Proceedings of the National Academy of Sciences* **2017**, 114, 5743.

[6] S.-i. Horigane, Y. Ozawa, H. Yamada, S. Takemoto-Kimura, *The Journal of Biochemistry* **2019**, 165, 401.

[7] N. Stafford, C. Wilson, D. Oceandy, L. Neyses, E. J. Cartwright, *Physiological reviews* **2017**, 97, 1089.

[8] T. Rodrigues, G. N. N. Estevez, I. L. dos Santos Tersariol, *Biochemical pharmacology* **2019**, 163, 357.

[9] C. Giorgi, A. Danese, S. Missiroli, S. Patergnani, P. Pinton, *Trends in cell biology* **2018**, 28, 258.

[10] A. M. Hofer, E. M. Brown, *Nature Reviews Molecular Cell Biology* **2003**, 4, 530.

[11] I. F. Smith, I. Parker, *Proceedings of the National Academy of Sciences* **2009**, 106, 6404.

[12] M. Fill, J. A. Copello, *Physiological reviews* **2002**, 82, 893.

[13] D. M. Anderson, C. A. Makarewich, K. M. Anderson, J. M. Shelton, S. Bezprozvannaya, R. Bassel-Duby, E. N. Olson, *Science signaling* **2016**, 9, ra119.

[14] K. Oxenoid, Y. Dong, C. Cao, T. Cui, Y. Sancak, A. L. Markhard, Z. Grabarek, L. Kong, Z. Liu, B. Ouyang, *Nature* **2016**, 533, 269.

[15] W. Huang, T. Wu, A. Shallan, R. Kostecki, C. K. Rayner, C. Priest, H. Ebendorff-Heidepriem, J. Zhao, *ACS Sensors* **2020**, DOI: 10.1021/acssensors.9b02308.

[16] P. Uhlén, N. Fritz, *Biochemical and biophysical research communications* **2010**, 396, 28.

[17] a) N. E. Ziv, M. E. Spira, *Journal of neurophysiology* **1995**, 74, 2625; b) J. Berlin, M. Cannell, W. J. Lederer, *Circulation research* **1989**, 65, 115; c) J. G. Danielczok, E. Terriac, L. Hertz, P. Petkova-Kirova, F. Lautenschläger, M. W. Laschke, L. Kaestner, *Frontiers in physiology* **2017**, 8, 979.

[18] a) B. F. Trump, I. K. Berezesky, *The FASEB journal* **1995**, 9, 219; b) S. K. Frandsen, H. Gissel, P. Hojman, T. Tramm, J. Eriksen, J. Gehl, *Cancer research* **2012**, 72, 1336.

[19] a) J. M. Borghans, G. Dupont, A. Goldbeter, *Biophysical chemistry* **1997**, 66, 25; b) L. Pasti, A. Volterra, T. Pozzan, G. Carmignoto, *Journal of Neuroscience* **1997**, 17, 7817; c) G. Hajnóczky, L. D. Robb-Gaspers, M. B. Seitz, A. P. Thomas, *Cell* **1995**, 82, 415; d) K. Samanta, G. R. Mirams, A. B. Parekh, *Nature communications* **2018**, 9, 1; e) K. Ishii, K. Hirose, M. Iino, *EMBO reports* **2006**, 7, 390; f) T. Wakai, N. Zhang, P. Vangheluwe, R. A. Fissore, *Journal of cell science* **2013**, 126, 5714.

[20] M. Endo, M. Tanaka, Y. Ogawa, *Nature* **1970**, 228, 34.

[21] K. Campbell, K. Swann, *Developmental biology* **2006**, 298, 225.

[22] J.-C. Henquin, *Diabetologia* **2009**, 52, 739.

[23] P. J. Hanley, B. Musset, V. Renigunta, S. H. Limberg, A. H. Dalpke, R. Sus, K. M. Heeg, R. Preisig-Müller, J. Daut, *Proceedings of the National Academy of Sciences* **2004**, 101, 9479.

[24] a) A. W. Simpson, *Calcium Signaling Protocols* **2013**, 3; b) J. Suzuki, K. Kanemaru, M. Iino, *Biophysical Journal* **2016**, 111, 1119; c) J. Suzuki, K. Kanemaru, M. Iino, *Biophys J* **2016**, 111, 1119; d) A. Takahashi, P. Camacho, J. D. Lechleiter, B. Herman, *Physiological reviews* **1999**, 79, 1089; e) K. P. Carter, A. M. Young, A. E. Palmer, *Chemical reviews* **2014**, 114, 4564.

[25] a) H. Dana, Y. Sun, B. Mohar, B. K. Hulse, A. M. Kerlin, J. P. Hasseman, G. Tsegaye, A. Tsang, A. Wong, R. Patel, *Nature methods* **2019**, 16, 649; b) M. Cerrone, J. Montnach, X. Lin, Y.-T.

Zhao, M. Zhang, E. Agullo-Pascual, A. Leo-Macias, F. J. Alvarado, I. Dolgalev, T. V. Karathanos, *Nature communications* **2017**, 8, 1; c) D. Huang, B. He, P. Mi, *Biomaterials science* **2019**, 7, 3942.

[26] a) O. Cabrera, D. M. Berman, N. S. Kenyon, C. Ricordi, P.-O. Berggren, A. Caicedo, *Proceedings of the National Academy of Sciences of the United States of America* **2006**, 103, 2334; b) A. Caicedo, presented at Seminars in cell & developmental biology **2013**.

[27] A. D. Association, *Diabetes Care* **2021**, 44, S15.

[28] a) T. Jensen, M. Kiersgaard, D. Sørensen, L. Mikkelsen, *Laboratory animals* **2013**, 47, 225; b) C. Sun, X. Li, L. Liu, M. Conet, Y. Guan, Y. Fan, Y. Zhou, *Int J Clin Exp Med* **2016**, 9, 4186.

[29] G. E. Anderson, Y. Kologlu, C. Papadopoulos, *Metabolism* **1967**, 16, 586.

[30] a) D. J. Koerker, C. J. Goodner, B. Walike Hansen, A. C. Brown, A. H. Rubenstein, *Endocrinology* **1978**, 102, 1649; b) J. I. Stagner, E. Samols, G. C. Weir, *The Journal of clinical investigation* **1980**, 65, 939; c) D. Lang, D. Matthews, J. Peto, R. Turner, *New England Journal of Medicine* **1979**, 301, 1023.

[31] N. Porksen, S. Munn, J. Steers, J. D. Veldhuis, P. C. Butler, *American Journal of Physiology-Endocrinology And Metabolism* **1995**, 269, E1106.

[32] N. Pørksen, *Diabetologia* **2002**, 45, 3.

[33] D. Matthews, B. Naylor, R. G. Jones, G. Ward, R. Turner, *Diabetes* **1983**, 32, 617.

[34] P. Bratusch-Marrain, M. Komjati, W. Waldhäusl, *Diabetes* **1986**, 35, 922.

[35] a) S. O'Rahilly, R. C. Turner, D. R. Matthews, *New England Journal of Medicine* **1988**, 318, 1225; b) J.-M. Lin, M. E. Fabregat, R. Gomis, P. Bergsten, *Diabetes* **2002**, 51, 988; c) B. Gumbiner, E. Van Cauter, W. F. Beltz, T. M. Ditzler, K. Griver, K. S. Polonsky, R. R. Henry, *The Journal of Clinical Endocrinology & Metabolism* **1996**, 81, 2061; d) S. J. Hunter, A. B. Atkinson, C. N. Ennis, B. Sheridan, P. M. Bell, *Diabetes* **1996**, 45, 683.

[36] a) F. M. Ashcroft, D. E. Harrison, S. J. Ashcroft, *Nature* **1984**, 312, 446; b) D. L. Cook, N. Hales, *Nature* **1984**, 311, 271.

[37] a) S.-N. Yang, P.-O. Berggren, *Endocrine reviews* **2006**, 27, 621; b) P. M. Dean, E. Matthews, *The Journal of physiology* **1970**, 210, 255.

[38] R. Jahn, D. Fasshauer, *Nature* **2012**, 490, 201.

[39] a) H. Kindmark, M. Köhler, G. Brown, R. Bränström, O. Larsson, P.-O. Berggren, *Journal of Biological Chemistry* **2001**, 276, 34530; b) P. Krippeit-Drews, M. Düfer, G. Drews, *Biochemical and biophysical research communications* **2000**, 267, 179.

[40] M. Balasubramanyam, L. P. Singh, S. Rangasamy, Hindawi, 2012.

[41] A. Gerbino, I. Maiellaro, C. Carmone, R. Caroppo, L. Debellis, M. Barile, G. Busco, M. Colella, *Cell calcium* **2012**, 51, 393.

[42] J.-C. Henquin, D. Dufrane, J. Kerr-Conte, M. Nenquin, *American Journal of Physiology-Endocrinology and Metabolism* **2015**, 309, E640.

[43] E. Grapengiesser, E. Gylfe, B. Hellman, *Biochemical and Biophysical Research Communications* **1988**, 151, 1299.

[44] a) M. Valdeolmillos, R. M. Santos, D. Contreras, B. Soria, L. M. Rosario, *FEBS letters* **1989**, 259, 19; b) I. Quesada, M. G. Todorova, P. Alonso-Magdalena, M. Beltrá, E. M. Carneiro, F. Martin, A. Nadal, B. Soria, *Diabetes* **2006**, 55, 2463.

[45] a) P. Bergsten, E. Grapengiesser, E. Gylfe, A. Tengholm, B. Hellman, *Journal of Biological Chemistry* **1994**, 269, 8749; b) J.-C. Jonas, P. Gilon, J.-C. Henquin, *Diabetes* **1998**, 47, 1266.

[46] a) A. I. Tarasov, F. Semplici, M. A. Ravier, E. A. Bellomo, T. J. Pullen, P. Gilon, I. Sekler, R. Rizzuto, G. A. Rutter, *PloS one* **2012**, 7, e39722; b) E. K. AINSCOW, G. A. RUTTER, *Biochemical Journal* **2001**, 353, 175.

[47] A. I. Tarasov, F. Semplici, D. Li, R. Rizzuto, M. A. Ravier, P. Gilon, G. A. Rutter, *Pflügers Archiv - European Journal of Physiology* **2013**, 465, 543.

[48] A. Wiederkehr, G. Szanda, D. Akhmedov, C. Mataki, C. W. Heizmann, K. Schoonjans, T. Pozzan, A. Spät, C. B. Wollheim, *Cell metabolism* **2011**, 13, 601.

[49] P. Gilon, H.-Y. Chae, G. A. Rutter, M. A. Ravier, *Cell calcium* **2014**, 56, 340.
[50] a) P. Gilon, A. Arredouani, P. Gailly, J. Gromada, J.-C. Henquin, *Journal of Biological Chemistry* **1999**, 274, 20197; b) A. Arredouani, J.-C. Henquin, P. Gilon, *American Journal of Physiology-Endocrinology and Metabolism* **2002**, 282, E982; c) A. Arredouani, Y. Guiot, J.-C. Jonas, L. H. Liu, M. Nenquin, J. A. Pertusa, J. Rahier, J.-F. Rolland, G. E. Shull, M. Stevens, *Diabetes* **2002**, 51, 3245.
[51] M. A. Ravier, D. Daro, L. P. Roma, J.-C. Jonas, R. Cheng-Xue, F. C. Schuit, P. Gilon, *Diabetes* **2011**, 60, 2533.
[52] K. Tornheim, *Diabetes* **1997**, 46, 1375.
[53] M. Ristow, H. Carlqvist, J. Hebinck, M. Vorgerd, W. Krone, A. Pfeiffer, D. Müller-Wieland, C.-G. Ostenson, *Diabetes* **1999**, 48, 1557.
[54] D. Li, S. Chen, E. A. Bellomo, A. I. Tarasov, C. Kaut, G. A. Rutter, W.-h. Li, *Proceedings of the National Academy of Sciences* **2011**, 108, 21063.
[55] E. M. Brown, G. Gamba, D. Riccardi, M. Lombardi, R. Butters, O. Kifor, A. Sun, M. A. Hediger, J. Lytton, S. C. Hebert, *Nature* **1993**, 366, 575.
[56] M. S. LeBoff, D. Shoback, E. M. Brown, J. Thatcher, R. Leombruno, D. Beaudoin, M. Henry, R. Wilson, J. Pallotta, S. Marynick, *The Journal of clinical investigation* **1985**, 75, 49.
[57] L. Komuves, Y. Oda, C. l. Tu, W. H. Chang, C. L. Ho‐Pao, T. Mauro, D. D. Bikle, *Journal of cellular physiology* **2002**, 192, 45.
[58] F. Lorget, S. Kamel, R. Mentaverri, A. Wattel, M. Naassila, M. Maamer, M. Brazier, *Biochemical and biophysical research communications* **2000**, 268, 899.
[59] A. M. Hofer, S. Curci, M. A. Doble, E. M. Brown, D. I. Soybel, *Nature Cell Biology* **2000**, 2, 392.
[60] C. E. Hills, M. Y. G. Younis, J. Bennett, E. Siamantouras, K. K. Liu, P. E. Squires, *Cellular Physiology and Biochemistry* **2012**, 30, 575.
[61] E. Gray, D. Muller, P. E. Squires, H. Asare-Anane, G.-C. Huang, S. Amiel, S. J. Persaud, P. M. Jones, *Journal of Endocrinology* **2006**, 190, 703.
[62] I. Kitsou-Mylona, C. J. Burns, P. E. Squires, S. J. Persaud, P. M. Jones, *Cellular Physiology and Biochemistry* **2008**, 22, 557.
[63] A. Calabrese, M. Zhang, V. Serre-Beinier, D. Caton, C. Mas, L. S. Satin, P. Meda, *Diabetes* **2003**, 52, 417.
[64] G. M. Grodsky, L. L. Bennett, Am Diabetes Assoc, 1966.
[65] P. Rorsman, P.-O. Berggren, E. Gylfe, B. Hellman, *Bioscience reports* **1983**, 3, 939.
[66] G. A. Rutter, J. Theler, M. Murgia, C. Wollheim, T. Pozzan, R. Rizzuto, *Journal of Biological Chemistry* **1993**, 268, 22385.
[67] A. Varadi, G. A. Rutter, *Diabetes* **2002**, 51, S190.
[68] L. Yi, B. Bandak, X. Wang, R. Bertram, M. G. Roper, *Analytical chemistry* **2016**, 88, 10368.
[69] E. B. Ridgway, C. C. Ashley, *Biochemical and biophysical research communications* **1967**, 29, 229.
[70] R. Y. Tsien, *Biochemistry* **1980**, 19, 2396.
[71] G. Grynkiewicz, M. Poenie, R. Y. Tsien, *Journal of Biological Chemistry* **1985**, 260, 3440.
[72] R. Rizzuto, A. W. Simpson, M. Brini, T. Pozzan, *Nature* **1992**, 358, 325.
[73] A. Miyawaki, J. Llopis, R. Heim, J. M. McCaffery, J. A. Adams, M. Ikura, R. Y. Tsien, *Nature* **1997**, 388, 882.
[74] O. Dyachok, O. Idevall-Hagren, J. Sågetorp, G. Tian, A. Wuttke, C. Arrieumerlou, G. Akusjärvi, E. Gylfe, A. Tengholm, *Cell metabolism* **2008**, 8, 26.
[75] H. Kindmark, M. Köhler, T. Nilsson, P. Arkhammar, K.-L. Wiechel, P. Rorsman, S. Efendić, P.-O. Berggren, *FEBS letters* **1991**, 291, 310.
[76] R. Y. Tsien, *Nature* **1981**, 290, 527.
[77] A. Moura, *Biochemical and biophysical research communications* **1995**, 214, 798.
[78] A. Verkhratsky, O. H. Petersen, *Calcium Measurement Methods*, Springer, **2010**.
[79] R. Tsien, T. Pozzan, *Methods in enzymology* **1989**, 172, 230.

[80] O. L. Barreto-Chang, R. E. Dolmetsch, *JoVE (Journal of Visualized Experiments)* **2009**, e1067.
[81] B. Valeur, M. N. Berberan-Santos, *Molecular fluorescence: principles and applications*, John Wiley & Sons, **2012**.
[82] P. Rorsman, H. Abrahamsson, E. Gylfe, B. Hellman, *FEBS letters* **1984**, 170, 196.
[83] a) F. Martin, B. Soria, *Cell calcium* **1996**, 20, 409; b) H. Kindmark, M. Köhler, P. Arkhammar, S. Efendic, O. Larsson, S. Linder, T. Nilsson, P. O. Berggren, *Diabetologia* **1994**, 37, 1121; c) B. Hellman, E. Gylfe, P. Bergsten, E. Grapengiesser, P. E. Lund, A. Berts, A. Tengholm, D. G. Pipeleers, Z. Ling, *Diabetologia* **1994**, 37, S11; d) Y. J. Liu, A. Tengholm, E. Grapengiesser, B. Hellman, E. Gylfe, *The Journal of physiology* **1998**, 508, 471; e) C. S. Nunemaker, R. Bertram, A. Sherman, K. Tsaneva-Atanasova, C. R. Daniel, L. S. Satin, *Biophysical journal* **2006**, 91, 2082; f) M. Zhang, P. Goforth, R. Bertram, A. Sherman, L. Satin, *Biophysical journal* **2003**, 84, 2852.
[84] M. C. Beauvois, C. Merezak, J.-C. Jonas, M. A. Ravier, J.-C. Henquin, P. Gilon, *American Journal of Physiology-Cell Physiology* **2006**, 290, C1503.
[85] a) D. S. Luciani, S. Misler, K. S. Polonsky, *The Journal of physiology* **2006**, 572, 379; b) J. Li, H. Y. Shuai, E. Gylfe, A. Tengholm, *Diabetologia* **2013**, 56, 1577.
[86] M. T. Spence, I. D. Johnson, *The molecular probes handbook: a guide to fluorescent probes and labeling technologies*, Live Technologies Corporation, **2010**.
[87] J.-I. Miyazaki, K. Araki, E. Yamato, H. Ikegami, T. Asano, Y. Shibasaki, Y. Oka, K.-I. YAMAMURA, *Endocrinology* **1990**, 127, 126.
[88] L. He, B. Dong, Y. Liu, W. Lin, *Chemical Society Reviews* **2016**, 45, 6449.
[89] J. Wu, W. Liu, J. Ge, H. Zhang, P. Wang, *Chemical Society Reviews* **2011**, 40, 3483.
[90] A. P. De Silva, H. N. Gunaratne, T. Gunnlaugsson, A. J. Huxley, C. P. McCoy, J. T. Rademacher, T. E. Rice, *Chemical reviews* **1997**, 97, 1515.
[91] D. Thomas, S. Tovey, T. Collins, M. Bootman, M. Berridge, P. Lipp, *Cell calcium* **2000**, 28, 213.
[92] S. Bassnett, L. Reinisch, D. C. Beebe, *American Journal of Physiology-Cell Physiology* **1990**, 258, C171.
[93] J. L. Perry, N. K. Ramachandran, B. Utama, J. M. Hyser, *Methods* **2015**, 90, 28.
[94] R. Rizzuto, A. W. Simpson, M. Brini, T. Pozzan, *Nature* **1992**, 358, 325.
[95] M. Nakazaki, H. Ishihara, M. Kakei, K. Inukai, T. Asano, J.-I. Miyazaki, H. Tanaka, M. Kikuchi, T. Yada, Y. Oka, *Diabetologia* **1998**, 41, 279.
[96] Z. Xia, J. Rao, *Current opinion in biotechnology* **2009**, 20, 37.
[97] A. E. Palmer, M. Giacomello, T. Kortemme, S. A. Hires, V. Lev-Ram, D. Baker, R. Y. Tsien, *Chemistry & biology* **2006**, 13, 521.
[98] J. Nakai, M. Ohkura, K. Imoto, *Nature biotechnology* **2001**, 19, 137.
[99] M. Mank, O. Griesbeck, *Chemical reviews* **2008**, 108, 1550.
[100] L. Filippin, M. C. Abad, S. Gastaldello, P. J. Magalhães, D. Sandonà, T. Pozzan, *Cell calcium* **2005**, 37, 129.
[101] O. Idevall-Hagren, S. Barg, E. Gylfe, A. Tengholm, *Journal of Biological Chemistry* **2010**, 285, 23007.
[102] D. Ammann, *Ion-selective microelectrodes: principles, design and application*, Springer Science & Business Media, **2013**.
[103] W. M. Kühtreiber, L. F. Jaffe, *The Journal of cell biology* **1990**, 110, 1565.
[104] G. Luxardi, B. Reid, F. Ferreira, P. Maillard, M. Zhao, *Journal of visualized experiments: JoVE* **2015**.
[105] E. Perez-Armendariz, I. Atwater, in *Biophysics of the Pancreatic β-Cell*, Springer **1986**, p. 31.
[106] M. Whitaker, *Calcium in living cells*, Academic Press, **2010**.
[107] M. Han, J. Zhao, J. M. Fabian, S. Evans, S. Mustafa, Y. Ruan, S. Wiederman, H. Ebendorff-Heidepriem, *ELECTROPHORESIS* **2021**, 42, 1247.
[108] S. Misler, Z. Zhou, A. S. Dickey, A. M. Silva, D. M. Pressel, D. W. Barnett, *Channels* **2009**, 3, 181.

[109] a) J. M. Kendall, R. L. Dormer, A. K. Campbell, *Biochemical and biophysical research communications* **1992**, 189, 1008; b) M. Brini, R. Marsault, C. Bastianutto, J. Alvarez, T. Pozzan, R. Rizzuto, *Journal of Biological Chemistry* **1995**, 270, 9896.
[110] A. E. Palmer, R. Y. Tsien, *Nature protocols* **2006**, 1, 1057.
[111] a) U. Schefer, D. Ammann, E. Pretsch, U. Oesch, W. Simon, *Analytical chemistry* **1986**, 58, 2282; b) K. Suzuki, K. Watanabe, Y. Matsumoto, M. Kobayashi, S. Sato, D. Siswanta, H. Hisamoto, *Analytical Chemistry* **1995**, 67, 324.
[112] H. He, K. Jenkins, C. Lin, *analytica chimica acta* **2008**, 611, 197.
[113] B. Sui, X. Liu, M. Wang, K. D. Belfield, *Chemistry-A European Journal* **2016**, 22, 10351.
[114] D. Rusakov, A. Fine, *Neuron* **2003**, 37, 287.
[115] F. Ishiwari, H. Hasebe, S. Matsumura, F. Hajjaj, N. Horii-Hayashi, M. Nishi, T. Someya, T. Fukushima, *Scientific reports* **2016**, 6.
[116] M. Gao, Y. Li, X. Chen, S. Li, L. Ren, B. Z. Tang, *ACS applied materials & interfaces* **2018**, 10, 14410.
[117] K. Takesako, K. Sasamoto, Y. Ohkura, K. Hirose, M. Iino, *Analytical Communications* **1997**, 34, 391.
[118] R. Zhan, Y. Pan, P. N. Manghnani, B. Liu, *Macromolecular bioscience* **2016**.
[119] M. Moirangthem, R. Arts, M. Merkx, A. P. Schenning, *Advanced Functional Materials* **2016**, 26, 1154.
[120] Y. Ding, J. Ling, Y. Qiao, Z. Li, Z. Sun, J. Cai, Y. Guo, H. Wang, *Scientific reports* **2016**, 6, 38602.
[121] E. S. Li, M. S. Saha, *Biomolecules* **2021**, 11, 343.
[122] S. Kim, J. W. Park, D. Kim, D. Kim, I. H. Lee, S. Jon, *Angewandte Chemie* **2009**, 121, 4202.
[123] D. Si, T. Epstein, Y.-E. K. Lee, R. Kopelman, *Analytical chemistry* **2012**, 84, 978.
[124] C. Yang, Y. Qin, D. Jiang, H.-y. Chen, *ACS applied materials & interfaces* **2016**, 8, 19892.
[125] M. Bagheri, M. Y. Masoomi, *ACS applied materials & interfaces* **2020**, 12, 4625.
[126] Y. Sun, Y. Xia, *science* **2002**, 298, 2176.
[127] A. J. Reynolds, A. H. Haines, D. A. Russell, *Langmuir* **2006**, 22, 1156.
[128] H. A. Clark, S. L. R. Barker, M. Brasuel, M. T. Miller, E. Monson, S. Parus, Z.-Y. Shi, A. Song, B. Thorsrud, R. Kopelman, A. Ade, W. Meixner, B. Athey, M. Hoyer, D. Hill, R. Lightle, M. A. Philbert, *Sensors and Actuators B: Chemical* **1998**, 51, 12.
[129] S. M. Buck, H. Xu, M. Brasuel, M. A. Philbert, R. Kopelman, *Talanta* **2004**, 63, 41.
[130] X. Hun, Z. Zhang, *Microchimica Acta* **2007**, 159, 255.
[131] L. B. Josefsen, J. W. Aylott, A. Beeby, P. Warburton, J. P. Boyle, C. Peers, R. W. Boyle, *Photochemical & Photobiological Sciences* **2010**, 9, 801.
[132] A. Webster, S. J. Compton, J. W. Aylott, *Analyst* **2005**, 130, 163.
[133] A. Schulz, R. Woolley, T. Tabarin, C. McDonagh, *Analyst* **2011**, 136, 1722.
[134] X. Xie, E. Bakker, *Analytical and bioanalytical chemistry* **2015**, 407, 3899.
[135] a) Y. Cui, Y. Yue, G. Qian, B. Chen, *Chemical reviews* **2012**, 112, 1126; b) B. Li, H. M. Wen, Y. Cui, W. Zhou, G. Qian, B. Chen, *Advanced Materials* **2016**, 28, 8819; c) L. E. Kreno, K. Leong, O. K. Farha, M. Allendorf, R. P. Van Duyne, J. T. Hupp, *Chemical reviews* **2012**, 112, 1105.
[136] D. J. Tranchemontagne, J. L. Mendoza-Cortés, M. O'Keeffe, O. M. Yaghi, *Chemical Society Reviews* **2009**, 38, 1257.
[137] W. P. Lustig, S. Mukherjee, N. D. Rudd, A. V. Desai, J. Li, S. K. Ghosh, *Chemical Society Reviews* **2017**, 46, 3242.
[138] W.-G. Lu, L. Jiang, X.-L. Feng, T.-B. Lu, *Inorganic chemistry* **2009**, 48, 6997.
[139] A. F. Adewola, D. Lee, T. Harvat, J. Mohammed, D. T. Eddington, J. Oberholzer, Y. Wang, *Biomedical microdevices* **2010**, 12, 409.
[140] P. N. Silva, B. J. Green, S. M. Altamentova, J. V. Rocheleau, *Lab on a Chip* **2013**, 13, 4374.
[141] T. Tao, Y. Wang, W. Chen, Z. Li, W. Su, Y. Guo, P. Deng, J. Qin, *Lab on a Chip* **2019**, 19, 948.
[142] P. Sokolowska, K. Zukowski, J. Janikiewicz, E. Jastrzebska, A. Dobrzyn, Z. Brzozka, *Biosensors and Bioelectronics* **2021**, 183, 113215.

[143] W.-H. Tan, S. Takeuchi, *Proceedings of the National Academy of Sciences* **2007**, 104, 1146.
[144] K. S. Sankar, B. J. Green, A. R. Crocker, J. E. Verity, S. M. Altamentova, J. V. Rocheleau, *PloS one* **2011**, 6, e24904.
[145] Y. Jun, J. Lee, S. Choi, J. H. Yang, M. Sander, S. Chung, S.-H. Lee, *Science Advances* **2019**, 5, eaax4520.
[146] T. Schulze, K. Mattern, E. Früh, L. Hecht, I. Rustenbeck, A. Dietzel, *Biomedical Microdevices* **2017**, 19, 47.
[147] S. Patel, M. Ishahak, D. Chaimov, A. Velraj, D. LaShoto, D. Hagan, P. Buchwald, E. Phelps, A. Agarwal, C. Stabler, *Science advances* **2021**, 7, eaba5515.
[148] a) T. Kin, P. Senior, D. O'Gorman, B. Richer, A. Salam, A. M. J. Shapiro, *Transplant International* **2008**, 21, 1029; b) H. Ichii, Y. Sakuma, A. Pileggi, C. Fraker, A. Alvarez, J. Montelongo, J. Szust, A. Khan, L. Inverardi, B. Naziruddin, M. F. Levy, G. B. Klintmalm, J. A. Goss, R. Alejandro, C. Ricordi, *American Journal of Transplantation* **2007**, 7, 1010.
[149] P. M. Misun, B. Yesildag, F. Forschler, A. Neelakandhan, N. Rousset, A. Biernath, A. Hierlemann, O. Frey, *Advanced biosystems* **2020**, 4, 1900291.
[150] R. Dhumpa, T. M. Truong, X. Wang, M. G. Roper, *Integrative Biology* **2015**, 7, 1061.
[151] S. Lu, C. E. Dugan, R. T. Kennedy, *Analytical chemistry* **2018**, 90, 5171.
[152] D. T. T. Nguyen, D. van Noort, I.-K. Jeong, S. Park, *Biofabrication* **2017**, 9, 015021.
[153] a) P. Thams, K. Capito, *Diabetologia* **2001**, 44, 738; b) J.-C. Henquin, *Diabetes* **2000**, 49, 1751.
[154] P. Newsholme, D. Keane, H. J. Welters, N. G. Morgan, *Clinical science* **2007**, 112, 27.
[155] C. Xie, K. L. Jones, C. K. Rayner, T. Wu, *Pharmaceutics* **2020**, 12, 790.
[156] W.-K. Huang, C. Xie, R. L. Young, J.-B. Zhao, H. Ebendorff-Heidepriem, K. L. Jones, C. K. Rayner, T.-Z. Wu, *World Journal of Gastroenterology* **2020**, 26, 3562.
[157] Y. Xing, M. Nourmohammadzadeh, J. E. M. Elias, M. Chan, Z. Chen, J. J. McGarrigle, J. Oberholzer, Y. Wang, *Biomedical microdevices* **2016**, 18, 80.
[158] Y.-J. Nam, Y. J. Yoon, S.-K. Lee, M. Im, J.-H. Park, *IEEE Sensors Journal* **2020**, 20, 14694.
[159] D. Agustini, M. F. Bergamini, L. H. Marcolino-Junior, *Biosensors and Bioelectronics* **2017**, 98, 161.
[160] a) X. Wang, L. Yi, M. G. Roper, *Analytical chemistry* **2016**, 88, 3369; b) J. G. Shackman, K. R. Reid, C. E. Dugan, R. T. Kennedy, *Analytical and bioanalytical chemistry* **2012**, 402, 2797.
[161] F. R. Castiello, K. Heileman, M. Tabrizian, *Lab on a Chip* **2016**, 16, 409.
[162] L. V. Heilbrunn, **1937**.
[163] M. Trebak, J.-P. Kinet, *Nature Reviews Immunology* **2019**, 19, 154.
[164] H. Bading, *Nature Reviews Neuroscience* **2013**, 14, 593.
[165] G. R. Monteith, N. Prevarskaya, S. J. Roberts-Thomson, *Nature Reviews Cancer* **2017**, 17, 367.
[166] M. W. Harr, C. W. Distelhorst, *Cold Spring Harbor perspectives in biology* **2010**, 2, a005579.
[167] S. Seino, K. Sugawara, N. Yokoi, H. Takahashi, *Diabetes, Obesity and Metabolism* **2017**, 19, 22.
[168] a) S. Speier, D. Nyqvist, O. Cabrera, J. Yu, R. D. Molano, A. Pileggi, T. Moede, M. Köhler, J. Wilbertz, B. Leibiger, *Nature medicine* **2008**, 14, 574; b) V. Salem, L. D. Silva, K. Suba, E. Georgiadou, S. N. M. Gharavy, N. Akhtar, A. Martin-Alonso, D. C. Gaboriau, S. M. Rothery, T. Stylianides, *Nature Metabolism* **2019**, 1, 615.
[169] C. A. Reissaus, A. R. Piñeros, A. N. Twigg, K. S. Orr, A. M. Conteh, M. M. Martinez, M. M. Kamocka, R. N. Day, S. A. Tersey, R. G. Mirmira, *Scientific reports* **2019**, 9, 1.
[170] S. Chen, Z. Huang, H. Kidd, M. Kim, E. H. Suh, S. Xie, E. H. Ghazvini Zadeh, Y. Xu, A. D. Sherry, P. E. Scherer, *Frontiers in Endocrinology* **2021**, 12, 118.

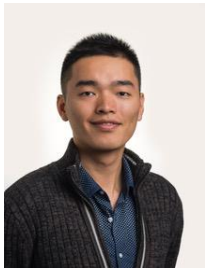

Weikun Huang has a Bachelor's degree in Veterinary Medicine (Jilin University, 2016), and a Master's degree in Physics (The University of Adelaide, 2019). In the latter, he developed substantial interests in the development of novel microfluidic bio-sensors for biomedical research. He is currently a PhD candidate at Adelaide Medical School, The University of Adelaide, focusing on the development of microfluidic sensing platforms for diabetes research.

Associate Professor Tongzhi Wu is a senior research fellow and a group leader within the Centre of Research Excellence in Nutritional Science at The University of Adelaide. His research concerns a broad range of fundamental and clinical topics relating to the pathophysiology and management of type 2 diabetes. He obtained his PhD at The University of Adelaide in 2013 with the award of a prestigious University Doctoral Research Medal, and established research leadership during his Royal Adelaide Hospital Mary Overton Early Career (2015-17) and Florey (2018-20) Fellowships. He is currently supported by a Mid-Career Fellowship from The Hospital Research Foundation (2020-23).

Professor Christopher Rayner is a Consultant Gastroenterologist at the Royal Adelaide Hospital, Australia. His major research interest concerns nutrient-gut interactions, including the regulation of gastrointestinal motility, with an emphasis on the role of upper gut function in diabetes. His key contributions have been to develop an understanding of the mechanisms of glucose sensing and incretin hormone release in the gut, and how these can be manipulated for therapeutic gain. He has developed the concept of protein preloads, taken in advance of meals, to initiate gut feedback mechanisms that will lower subsequent postprandial glycaemia in type 2 diabetes.

Professor Heike Ebendorff-Heidepriem is Deputy Director of the Institute for Photonics and Advanced Sensing (IPAS) and Director of the Optofab Adelaide Hub at the Australian National Fabrication Facility (ANFF). She obtained her PhD in chemistry from the University of Jena, Germany in 1994. Her research focuses on the development of novel optical glasses, fibres, surface functionalization and sensing approaches.

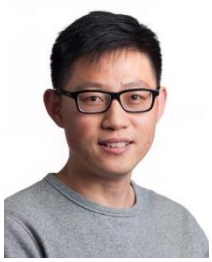

Dr Jiangbo (Tim) Zhao obtained his PhD degree from Macquarie University, Australia, followed by post-doctoral training at The University of Adelaide, Australia (2015-17) and at the Leibniz Institute of Photonic Technology, Jena, Germany (2018-19) with support of Alexander von Humboldt Fellowship. In 2021 he commenced as a lecturer at the University of Hull, UK. Dr Zhao's research enthusiasm revolves around materials physics and chemistry, including light-matter interaction as well as ensuing applications, e.g., biomedical research.

This review describes the development and current status of Ca^{2+} sensors in tracing intra- and extracellular Ca^{2+}, with a focus on the relevance of Ca^{2+} signalling to insulin secretion in the islet of Langerhans. Insights into Ca^{+} sensors have a high potential to facilitate their advancement towards improved understanding of the molecular mechanisms underpinning cellular functions.

W. H., T. W.,* C. X., C. K. R., C. P., H. E., J. (T.) Z.*

ToC figure

Sensing intra- and extracellular Ca^{2+} in the islet of Langerhans